WATER DROP DEFORMATION AND FRAGMENTATION DUE TO SHOCK WAVE IMPACT

By
WILLIAM EDWARD KRAUSS

A DISSERTATION PRESENTED TO THE GRADUATE COUNCIL OF
THE UNIVERSITY OF FLORIDA
IN PARTIAL FULFILLMENT OF THE REQUIREMENTS FOR THE
DEGREE OF DOCTOR OF PHILOSOPHY

UNIVERSITY OF FLORIDA
1970

To my wife

Barbara

for her patience, understanding

and encouragement

ACKNOWLEDGEMENTS

The author is indebted to many individuals for aid and encouragement in the completion of this dissertation. He wishes to express his gratitude to his fellow students and the faculty of the Aerospace Department of the University of Florida for their aid and suggestions during the course of the research work. In particular, the author wishes to thank Messrs. Tom McRae, Jerry Ward, Ron Brunsvold, Donald Dietrich, John Fisher and George Perdue for their assistance in preparing and conducting the experiment.

Special thanks are due to his supervisory committee chairman, Dr. B. M. Leadon, who has served with great understanding as a teacher, mentor, and critic. The author wishes to express his appreciation to members of his supervisory committee, Dr. M. H. Clarkson, Dr. D. T. Williams, Dr. R. K. Irey, and Dr. R. G. Blake.

The author also wishes to thank Mrs. Nancy Bryan, who graciously and ably prepared this manuscript.

Finally the author wishes to thank the Martin Marietta Corporation and, in particular, Mr. R. Dewey Rinehart, and Mr. John Calathes who sponsored the Doctoral Research Award which provided the financial support for completion of this research.

TABLE OF CONTENTS

LIST OF TABLES

LIST OF FIGURES

NOMENCLATURE

a	=	Dimensionless semi-minor axis of ellipsoid $(\tilde{a}/D)$, speed of sound $(\tilde{a}/\beta\tilde{U}_2)$
$\tilde{a}$	=	Semi-minor axis of ellipsoid, speed of sound
B	=	Dimensionless diameter of equator $(2b)$
b	=	Dimensionless semi-major axis of ellipsoid $(\tilde{b}/D)$
$\tilde{b}$	=	Semi-major axis of ellipsoid
C_p	=	Pressure coefficient
D	=	Initial diameter of drop
F	=	Dimensionless force $(\tilde{F}/\rho_\ell \beta^2 \tilde{U}_2^2 D^2)$
$\tilde{F}$	=	Force
f	=	Dimensionless function
M_R	=	Relative Mach number of drop $(\tilde{U}_2 - W)/a_2$
M_S	=	Shock wave Mach number
m	=	Dimensionless mass of drop $(\tilde{m}/\rho_\ell D^3)$
$\tilde{m}$	=	Mass of drop
p	=	Dimensionless static pressure $(\tilde{p}/\rho_\ell \tilde{U}_2^2 \beta^2)$
$\tilde{p}$	=	Static pressure
q	=	Dimensionless dynamic pressure $(\tilde{q}/\rho_\ell \tilde{U}_2^2 \beta^2)$
$\tilde{q}$	=	Dynamic pressure
R_μ	=	Ratio of viscosities
R	=	Dimensionless radius $(\tilde{R}/D)$
$\tilde{R}$	=	Radius
T	=	Dimensionless time $(t\beta\tilde{U}_2/D)$
T_B	=	Dimensionless time for shock wave to pass over drop
T_{sep}	=	Dimensionless time for boundary layer separation
t	=	Time after impact

u,v,w = Dimensionless velocities

U = Dimensionless velocity of fluid $(\tilde{U}/\tilde{U}_2\beta)$

$\tilde{U}$ = Velocity of fluid

W = Dimensionless velocity of drop

x,y,z = Dimensionless coordinates

X = Dimensionless displacement of drop $(\tilde{X}/D)$

$\tilde{X}$ = Displacement of drop

α = Dimensionless acceleration, Boundary layer shape factor

β = Density ratio $(\rho_2/\rho_\ell)^{1/2}$

δ = Dimensionless boundary layer thickness

ϵ = Eccentricity $(1-a^2/b^2)^{1/2}$

ζ,η = Dimensionless boundary layer coordinates

θ = Eccentric angle of ellipse

ν = Dimensionless kinematic viscosity of fluid $(\tilde{\nu}/D\beta\tilde{U}_2)$

$\tilde{\nu}$ = Kinematic viscosity of fluid

μ = Viscosity of fluid

ξ = Dimensionless coordinate

ρ = Density of fluid

σ = Dimensionless surface tension $(\tilde{\sigma}/\rho_\ell D\beta^2\tilde{U}_2^2)$

$\tilde{\sigma}$ = Surface tension

τ = Dimensionless time for one oscillation of drop, dimensionless shear stress

ϕ = Angle, velocity potential

SUBSCRIPTS

1 = Condition upstream of shock wave

2 = Condition downstream of shock wave

d = Drop

i = Initial

I = Interface

i,j = Computation indices

L = Stagnation Point

	=	Liquid, lost, local
m	=	Condition at maximum
o	=	Stagnation condition
p	=	Point at which pressure is acting
∞	=	Condition in free stream

Abstract of Dissertation Presented to the Graduate Council
in Partial Fulfillment of the Requirements for the
Degree of Doctor of Philosophy

WATER DROP DEFORMATION AND FRAGMENTATION DUE TO SHOCK WAVE IMPACT

By

William Edward Krauss

June, 1970

Chairman: B. M. Leadon
Major Department: Aerospace Engineering

Results are presented of experimental and theoretical studies of water drop deformation and fragmentation in the high velocity air stream following a normal shock wave moving into still air. Experiments were conducted in a shock tube with shock wave Mach numbers in the range from 1.6 to 3.0 and for drop diameters from .5 to 3.2 millimeters. From the experimental data, it is determined that the water drop deforms axisymmetrically into an approximately ellipsoidal shape which is distorted as to maintain a nearly hemispherical frontal surface but with a concave rear surface. The data also indicate that the time for complete fragmentation of the water drop is approximately one-half of the time observed for complete reduction of the drop to a trace of mist.

Simultaneous potential flow within the distorted ellipsoidal drop and mass loss by stripping of a viscous layer of surface liquid are included in a theoretical model for drop deformation and fragmentation. Although the actual drop deformation is shown to deviate from the assumed ellipsoidal shape, the general dimensional and displacement variations are predicted by the model and the theoretical mass history of the drop agrees well with the experimental data.

CHAPTER I

INTRODUCTION

The deformation and fragmentation of water drops caused by sudden exposure to a high velocity air stream currently has important application in the field of missile and aircraft structural and heat shield design. Rain erosion by the impingement of rain drops on the exterior surfaces of missiles causes severe damage to ablative heat shields and may result in structural failure of the missile. The effects of erosion damage can perhaps be minimized by judicious selection of the heat shield material to withstand drop impact or by suitable aerodynamic design of the missile. In this latter approach, the missile nose cap may be designed to generate a shock wave with a standoff distance sufficiently large to permit drop fragmentation before impingement upon the heat shield. Either of these approaches for minimizing rain erosion damage requires knowledge of rain drop size and shape as function of time.

Fragmentation of liquid drops in high velocity gas streams also occurs in fuel injection systems. The rates of mixing and of combustion in such systems are significantly enhanced by drop fragmentation.

A comprehensive literature survey was conducted on liquid drop deformation and fragmentation. Two modes of drop fragmentation which occur are related to Weber's number. The first of these modes occurs when the velocity of the gas stream relative to the drop is small and corresponds to a magnitude of Weber's number of from 1 to 10 or

20 times its critical value. In this mode of fragmentation, the drop is deformed into a "bag" shape prior to fragmentation. The second mode of fragmentation occurs when the velocity of the gas stream relative to the drop is high and corresponds to the case of Weber's number being very much greater than the critical value for drop fragmentation. In this mode the drop is deformed axisymmetrically and is fragmented by the stripping of a liquid layer from its surface.

The second mode of fragmentation is of interest for the present study; therefore, only those papers in the literature which are relevant to the second mode of fragmentation are discussed.

In general, the approach taken by all investigators has been similar in that each used photographic techniques to measure drop deformation and fragmentation in the gas stream behind a normal shock wave in a shock tube. Quantities measured were drop diameter, drop displacement and shock wave Mach number. Appropriate values of liquid density, viscosity and surface tension and of gas density and temperature were noted.

Engel[1] conducted comprehensive studies wherein the parameters varied were water drop size and shock wave Mach number. These were the first studies to show that drop fragmentation is not caused by the initial impact of the shock wave on the drop. In addition, these were the first studies to show deformation of the drop into a lenticular shape and stripping of a liquid surface layer from the drop. Engel considers several phenomena which might explain the stripping action but reaches no clear conclusion as to the cause of stripping. In addition, an approach which defines drop deformation based on potential flow within the drop is suggested.

Studies by Hanson, et al.[2] were conducted on very small drops (0.5 mm diameter) of various liquids. Shock wave Mach number was again varied but, as in Engel's[1] studies, did not exceed approximately 1.7. These studies verified Engel's observations on larger drops.

Nicholson and Figler[3] conducted the first studies with shock wave Mach numbers greater than 2 thereby producing a supersonic air velocity behind the shock wave. This was accomplished by using sub-atmospheric pressures in the driven section of the shock tube. The stripping phenomenon was again observed. Drop fragmentation was shown to depend largely on the dynamic pressure which was acting on the drop. An empirical correlation for the time required to achieve complete drop fragmentation is presented using the data developed for this study as well as those available from Engel and Hanson, et al.

The studies of Ranger and Nicholls[4] were conducted on water drops having diameters of .75 to 4.0 mm. Shock wave Mach numbers from 1.5 to 3.5 in air were used to extend the work of previous investigators. Dynamic pressures achieved were significantly greater than those of Nicholson because the pressure in the driven section of the shock tube for these studies was one atmosphere. The drop was observed to assume an ellipsoidal shape during deformation, and mass removal was attributed to boundary layer stripping. Using empirical relations for drop diameter and drop relative velocity, the validity of Taylor's[5] boundary layer stripping analysis was investigated. Based on the assumption of incompressible flow using approximate relations for the experimental data, the authors concluded that the agreement between Taylor's analysis and their experimental data was encouraging.

In the following chapters are reported the results of similar measurements which were being started as the Ranger and Nicholls[4] paper appeared in the literature. This is followed by an analytical treatment of simultaneous deformation and fragmentation of the drop and by a comparison of the experimental results with the analysis.

CHAPTER II

EXPERIMENTAL INVESTIGATION

Experimental Apparatus

The experimental arrangement used for this investigation is shown in Figure 1. A stream of water drops was injected by means of hypodermic needles into a shock tube test section which contained photographic windows. Figures 2 and 3 show, respectively, the water drop injectors and the test section. The drops fell vertically into the test section which was open to the atmosphere. Initial pressure in the test section was one atmosphere. The basic shock tube as described by Clemons[6] was modified by increasing the driver length to 36 inches. This was necessary to ensure that there was sufficient time for complete drop fragmentation prior to the arrival of the expansion wave.

Both helium and air were used as driver gases. A model 600 Honeywell Strobnar photographic flash unit was used to back light the drops as is shown in Figure 4. A model 1D TRW[7] image converter camera was employed to photograph the drops after shock wave impact. The image converter camera was electronically triggered by a platinum film velocity gauge[8] located a known distance from a fiducial marker scribed on the test section window. In addition, one window contained a millimeter grid which was used during data reduction to establish initial drop diameter. The experimental procedure consisted of obtaining a history of the deformation and displacement of an individual drop by taking a series of shadow photographs at various time intervals

after the shock wave impinged upon the drop. The timing sequence was set by a combination of TRW trigger delay generators,[9] Techtronix oscilloscopes,[10] and delay circuits as shown in Appendix I.

Data Reduction

The individual photographs were first examined with a Gaertner optical micrometer to establish a history of the displacement and major diameter variation of the drop. The time at which the first picture was taken was established by calculating the time required for the shock wave to travel from the velocity gauge to the drop whose initial position relative to the fiducial marker was recorded on the first photograph. The time interval between subsequent photographs was established by the intervals manually set into the timing circuit. Following initial examination of the photographs with the optical micrometer, the photographs were enlarged with a Beseler Vu-Lyte III opaque projector and measurements were made to determine the shape of the windward surface of the drop.

Data Analysis and Results

The results discussed here are for experiments that cover the shock wave Mach number range of M_S = 1.6 to 3.0 in air with drops having diameters in the range D = 0.5 to 3.2 millimeters. Deformation and displacement data obtained from photographs were reduced in terms of dimensionless displacement, X_L, dimensionless semi-major diameter, b, dimensionless semi-minor diameter, a, and dimensionless time, T.

Typical image converter camera photographs of shock wave-water drop interactions are shown in Figure 5. The dimensionless and corresponding real times at which the exposures were made are shown in Table I. Figure 5a, exposure 5, Figure 5b, exposure 3 and Figure 5c, exposure 2 show the drops

at approximately their maximum deformation which, from Table I, is seen to occur in the time interval T = 1.4 to 1.8. Figure 5b exposure 5 and Figure 5c exposure 4 show similar stages of drop fragmentation and indicate that while time T is similar, actually, in real time, the smaller drop shatters much more rapidly than the larger drop.

Two stages of development can be observed in the deformation and fragmentation process. During the first stage, deformation by flattening and curving is the primary phenomenon observed with little or no fragmentation in the form of mist visible. Deformation into a curved axisymmetrical ellipsoid is the result of the external pressure distribution on the drop. The second stage is characterized primarily by a surface stripping action which is due to the shearing action of the external flow field. This shearing action rapidly reduces the drop to a cloud of finely divided particles which will be termed "micromist." The second stage is well established by T = .20.

From Figure 5 it is seen that a well defined wake is formed behind the drop during early stages of fragmentation. The shape of this wake is similar to that developed behind a hypersonic blunt body where the flow converges because of strong lateral pressure gradients to form a recompression neck region several body diameters downstream from the rear stagnation point. This phenomenon was also observed by Ranger and Nicholls.[4] Since the liquid surface layer which is continuously being stripped from the drop is able to follow the streamline pattern of the wake, it is reasonable to conclude that the stripped liquid is composed of very fine water particles, a micromist. If large pieces of liquid were being stripped from the drop, the inertia of these pieces would preclude their following the stream lines and a significantly

different wake shape would be observed in the photographs. Figure 5c and other similar photographs which show considerable portions of the wake indicate that fragmentation is a continuous process which ultimately reduces the entire drop to a micromist cloud.

Taking the time for complete drop fragmentation to be that to leave only a trace of mist, as was done by Engel[1] and other investigators, curves of the deformation of the drop and the displacement of the drop were obtained and are shown in Figures 6 and 7, respectively, as functions of dimensionless time, T. These figures also include a band which indicates the range of experimental data available in the literature. It is seen that the data of this study agree well with those of other investigators. Figure 6 indicates that complete fragmentation of the drop occurs at approximately T = 5.0 as was also found by others.

Examination of the enlargements of the photographs obtained with the opaque projector indicated that significant irregularities occur in the windward surface of the drop at dimensionless times between approximately T = 2.0 and T = 2.5 and suggests that a breakup criterion other than reduction of the drop to a trace of mist might be identified. Measurements made on the windward surface of the drop in the various photographs using the parameters as shown in Figure 8 indicate this surface is approximately that of an axisymmetrical ellipsoid, the eccentricity of which varies with time as shown in Figure 9. These data were fitted with a mean fifth degree curve of least mean square deviation expressed by

$$\epsilon = 3.432T - 6.515T^2 + 4.656T^3 - 1.477T^4 + .1753T^5 \qquad \text{(II-1)}$$

Figure 9 shows the eccentricity varies from 0 to a maximum of .59 and returns to 0. The frontal surface changes from

that of a sphere to that of an axisymmetric ellipsoid and returns to the spherical surface shape. The measured maximum diameter of the drop and the measured displacement of the stagnation point of the drop were fitted with least mean square curves given by

$$B = 1 + 2.615T - .6776T^2 - .0971T^3 \qquad \text{(II-2)}$$

and

$$X_L = .409T^2 + .317\,T^3 \qquad \text{(II-3)}$$

and are shown in Figures 10 and 11, respectively.

The fitted curve for the displacement, Equation (II-3), also satisfies the known conditions at T = 0 that the dimensionless velocity of the drop is zero and the dimensionless acceleration is .818. The dimensionless acceleration is, of course, readily calculated for a sphere with a known pressure distribution. Details of this calculation as well as a method for determining the pressure distribution on axisymmetrical ellipsoidal bodies are presented in Chapter III.

The dimensionless mass, m, of the drop and the thickness, $2a_d$, of the drop were estimated by dividing the drop into annular elements of fixed thickness Δy and fixed radius y and applying Newton's Second Law to each element. The dimensionless force acting on an element is given by

$$F = 2\pi y \,\Delta y \,\Delta p \qquad \text{(II-4)}$$

where p is the pressure acting on the element at radius y_p. The dimensionless mass of the cylindrical element is given by

$$m = 4\pi y \,\Delta y x_d \qquad \text{(II-5)}$$

At time T the dimensionless location of the element with respect to the fiducial marker is given by

$$X_p = X_L + \zeta_p \qquad \text{(II-6)}$$

which in terms of the eccentricity and equation for an ellipse can be written as

$$X_p = X_L + b\,(1-\epsilon^2)^{\frac{1}{2}} \left\{ 1 - \left[1-(y_p/b)^2 \right]^{\frac{1}{2}} \right\} \qquad \text{(II-7)}$$

Since X_L, ϵ and b are known functions of time, T, as given by equations (II-1), (II-2), and (II-3), and since y_p is known for any element, the acceleration of the element at any time, T, can be found by differentiating equation (II-7) twice with respect to T. Making the substitutions noted and performing the differentiation, the dimensionless acceleration, $\ddot{X}_p$, of the element is given by

$$\begin{aligned}\ddot{X}_p = \ddot{X}_L &+ (\ddot{b}E + 2\dot{b}\dot{E} + b\ddot{E})(1-\Phi) \\ &+2\dot{b}\dot{E}(\Phi^2-1)/\Phi - \dot{b}^2 E(\Phi^2-1)/\Phi b \\ &+\ddot{b}E(\Phi^2-1)/\Phi + \dot{b}^2E(\Phi^2-1)^2/\Phi^3 b\end{aligned} \qquad \text{(II-8)}$$

where $E = (1-\epsilon^2)^{\frac{1}{2}}$

$\Phi = \{1-(y_p/b)^2\}^{\frac{1}{2}}$

Applying Newton's Second Law and using equations (II-4), (II-5), and (II-7), the dimensionless thickness of the element is given by

$$a_d = \Delta p/2 \ \ddot{X}_p \qquad \text{(II-9)}$$

The dimensionless total mass of the drop is readily found by summing the masses of the elements as found by equation (II-5).

Figure 12 presents the dimensionless semi-minor axis of the drop, a_d, and the measured semi-minor axis, a, of the surface visible in the photographs which is hereafter called the frontal surface. The water drop itself is deformed into a curved ellipsoid which has the observed frontal surface but a rearward surface which is increasingly concave. The axis of the axial section of this curved ellipsoid is calculated from the data. The semi-minor axis a_d is calculated as indicated above, and the semi-major axis b_d is measured along the locus of centroids of the cylindrical segments whose lengths have been calculated and plotted in Figures 13-24.

Figure 25 presents the semi-major axis of the drop as a function of dimensionless time, T, and Figure 26 presents the eccentricity of the drop as a function of T also. Comparison of Figures 10 and 25 shows the semi-major axis of both the

frontal surface and the drop reach maximum values at approximately T = 1.5. Figure 24 shows the cross section of the forward portion of the frontal surface and the deformation of the water drop as determined by the solution of equations (II-4) through (II-9) for various values of T. This figure shows the water drop deforms into an axisymmetric body which is crescent shaped, or curved elliptical, in cross section. The semi-minor axis of the curved ellipse decreases with time as mass is lost from the drop.

Figure 27 presents the velocity of the stagnation point of the drop. The velocity of the stagnation point is given by

$$W_L = .818T + .951T^2 \qquad \text{(II-10)}$$

which is directly obtained by differentiation of equation (II-3).

Figure 28 presents the dimensionless mass of the drop normalized to its initial mass and shows that the mass of the drop is reduced to approximately 2 percent of its initial mass by time T = 2.5 and indicates that for all practical engineering purposes drop breakup is complete at approximately this time. This result indicates the drop is fragmented in approximately one half the time for breakup as found by using the criterion that the drop is reduced to only a trace of mist as observed on photographs.

Experimental Error

During the experiment, shock tube driver pressures were measured within $\pm$3.5 percent with a Heise model C-55950 pressure gauge, temperatures within $\pm$1.5 percent and velocity of the shock wave within $\pm$3.0 percent.[8] Time intervals between photographic exposures were established by use of the time delay circuits in the Tektronix oscilloscopes which have an

accuracy of $\pm$2 percent of full scale and the time delay circuits in the TRW trigger pulse generators which have an accuracy of 0.01 percent of full scale.[9]

Repeated measurements made with the optical micrometer indicated that distances between two points, e.g., between the fiducial marker and the forward stagnation point of the drop, could be measured within $\pm$3.5 percent. Comparison of identical measurements made on the photographs using the optical micrometer with those made on the enlargements of the photographs indicate that the latter measurements were accurate to within $\pm$7 percent.

The standard deviations associated with each set of experimental data which were fitted with least mean square curves are shown in Figure 9, 10 and 11 and are .041, .095, and .112 for the eccentricity, the semi-major diameter of the front surface, b, and the displacement of the stagnation point, X_L, respectively. Since the standard deviation is the most probable expected error, it is indicative of the error due to curve-fitting the data. The standard deviation of the displacement curve, Figure 11, and the associated equation, (II-3), are of particular interest since equation (II-3) is differentiated to find the velocity and acceleration of the stagnation point of the drop. The maximum standard deviations for the velocity and the acceleration are calculated to be .124 and .146 respectively. Therefore, based on the average acceleration of the drop over the period T = 0 to T = 2.5, the calculated mass of the drop is accurate to within $\pm$10 percent.

CHAPTER III

THEORY

General

For convenience the analysis is divided into two parts. In the first part, the passage of the shock wave over the drop, the velocity and displacement of the water drop are mathematically characterized assuming the flow remains attached to the drop as the shock wave passes over it. No fluid motion within the drop is assumed to occur. This latter assumption appears to be justified, based on the photographic data of Engel.[1] In addition, for the conditions of this study the natural period, τ , for steady oscillation of the drop under surface tension as given by Rayleigh,[11]

$$\tau = 2\pi \left\{ 2\sigma n(n-1)(n+2) \right\}^{\frac{1}{2}}$$

is at least three orders of magnitude greater than the time

$$T_B = (2U_1)^{-1}$$

for the shock wave to pass over the drop.

The second part of the analysis considers drop deformation and fragmentation and begins when the shock wave reaches the rearmost point on the surface of the spherical drop. The flow field around the drop and the boundary layer are assumed to be fully established. Considering the time required for the boundary layer to become established as approximately that required for boundary separation to take place, it is found from Schlichting[12] that

$$T_{sep} = .196\beta$$

The maximum dimensionless separation time for the conditions of this study is $T_{sep} = 1.34 \times 10^{-2}$. This is also the time

required for the shock wave to move approximately a quarter of a body diameter; thus, the assumption of a fully established boundary layer appears to be reasonable.

Potential flow within the drop is assumed, and deformation of the drop is assumed to occur in a manner similar to that suggested by Engel.[1] The analysis here, however, is assumed not to be limited to small changes in the drop radius. Stripping of a liquid layer from the surface of the drop as suggested by Taylor[5] is also assumed. These two flow mechanisms are combined in a model which undergoes simultaneous drop deformation and mass loss. Axial symmetry is assumed throughout the analysis.

The analyses are developed in terms of non-dimensional variables and reduced to numerical solution by the standard forward marching technique used on high speed electronic computers. The necessity for computer solution is discussed as the analysis is developed.

Passage of Shock Wave Over the Drop

The coordinate systems used to define the position of the shock wave, the drop velocity, and the drop displacement are shown in Figure 29. The force acting on the drop at time T is:

$$F = .25\pi \int_0^{\Phi(T)} q_2 C_{pm} \left\{ (1-K_2) \sin^2\phi(T) - .28 \sin^4\Phi(T) \right\} d\phi(T) \qquad \text{(III-1)}$$

where q_2, C_{pm}, K_2 and are functions of T. K_2 is a parameter which governs the difference between the pressure ahead of and behind the shock wave as it moves over the drop and is given by

$$K_2 = 1.166 \, (1-M_S^2) \, p_1/q_2 C_{pm}$$

Since the dimensionless mass of the drop is

$$m = \frac{\pi}{6}$$

the drop acceleration can be found from Newton's Second Law provided the parameters under the integral sign in equation (III-1) are known functions of time. Since this is not the case, a forward marching numerical solution is employed wherein the increment $\Delta\phi$ is taken sufficiently small such that q_2, C_{pm} K_2 and ϕ can be assumed with small error to be constant within the interval ϕ to $\phi+\Delta\phi$. A substantial cumulative error may be incurred with this process, of course, but this is not investigated here because the objective is only to estimate the drop deformation and displacement which occur during the shock passage time. The drop acceleration is then found to be:

$$\alpha = 1.5 q_2 C_{pm} \int_{\phi}^{\phi+\Delta\phi} \left\{ (1-K_2) \sin^2\phi - .28 \sin^4\phi \right\} d\phi \qquad \text{(III-2)}$$

The drop velocity and displacement are found in the usual manner by integration with the initial conditions $\alpha = W = X_L = 0$ at $T = 0$. Using $\Delta\phi$ to set the computation interval, the corresponding time interval is:

$$\Delta T_i = \frac{X_i - .5\cos\Delta\phi}{a_1 M_s} \qquad \text{(III-3)}$$

and the velocity and displacement of the drop center are given, respectively, by:

$$W_i = \sum_{j=1}^{i} \left(\alpha_j \Delta T_j + W_{j-1} \right) \qquad \text{(III-4)}$$

and

$$X_i = \sum_{i=1}^{j} \left(W_i + \frac{\alpha_i \Delta T_i}{2} \right) \Delta T_i \qquad \text{(III-5)}$$

The maximum pressure coefficient is given by

$$C_{pm} = 1.4 + \frac{|M_R - .7| - |M_R - 1.3|}{1.5} \qquad \text{(III-6)}$$

where for subsonic flow C_{pm} is unity. C_{pm} is approximated by a linear increase from $C_{pm} = 1.0$ to $C_{pm} = 1.8$ for $.7 \leq M_R \leq 1.3$ and by $C_{pm} = 1.8$ for $M_R > 1.3$. The value of $C_{pm} = 1.8$ is typical of that found experimentally by numerous investigators.

Drop Deformation and Fragmentation

The coordinate systems used in this part of the analysis are shown on Figures 8 and 30. The drop is assumed to be an axisymmetric ellipsoid which has been distorted so that the front surface is spherical in shape. The (X,Y) coordinate system is fixed in space while the z, ξ, y-coordinate system is body-fixed and ζ, η are the coordinates fixed in the boundary layer. Assuming that potential flow exists internally in the drop, let the components of velocity of any liquid particle in the body-fixed coordinate system be

$$u = -2f\xi \qquad \text{(III-7a)}$$

$$v = fy \qquad \text{(III-7b)}$$

$$w = fz \qquad \text{(III-7c)}$$

where f is an undetermined function of time and is zero at $T = 0$. Based on the assumption of potential flow, there exists a velocity potential

$$\phi = .5f(-2\xi^2 + y^2 + z^2) \qquad \text{(III-8)}$$

such that

$$\frac{\partial \phi}{\partial \xi} = -2f\xi \qquad \text{(III-9a)}$$

$$\frac{\partial \phi}{\partial y} = fy \qquad \text{(III-9b)}$$

$$\frac{\partial \phi}{\partial z} = fz \qquad \text{(III-9c)}$$

Equations (III-7) and (III-9) clearly satisfy the continuity equation assuming no mass loss from the drop. Taking the term $.5(u^2 + v^2 + w^2)$ to be small and integrating the equation of motion the pressure is found to be given by

$$p = \frac{\partial \phi}{\partial T} + C(T) \qquad \text{(III-10)}$$

Applying equation (III-10) at the stagnation point, $\xi = -a_d$, and at the equator, $y = b_d$, of the drop, the following relationship is obtained:

$$\dot{f} = \frac{\Delta p}{a_d^2 + .5 b_d^2} \qquad \text{(III-11)}$$

where Δp is the pressure difference between the points $\phi = \pi$ and $\phi = \pi/2$ on the spherical surface of the drop. All parameters in equation (III-11) are unknown functions of time; hence, appeal is again made to a numerical solution where the computation interval is sufficiently small to assure that the equation

$$\Delta f = \frac{\Delta p \Delta T}{a_d^2 + .5 b_d^2}$$

is valid with negligible error. The function f may therefore be constructed as

$$f_j = \sum_{i=1}^{j} \left(\frac{\Delta p \Delta T}{a_d^2 + .5 b_d^2} \right)_i \qquad \text{(III-12)}$$

Since $+2fa_d$ is the velocity of the point (-a,o,o) on the surface of the axisymmetric ellipsoid,

$$\frac{\xi^2}{a_d^2} + \frac{y^2}{b_d^2} + \frac{z^2}{b_d^2} = 1 \qquad \text{(III-13)}$$

a new value for the semi-minor axis, a_d, at the end of the computational interval is readily determined from:

$$(a_d)_i = (a_d)_{i-1}(1 - 2f_i \Delta T_i) \qquad \text{(III-14)}$$

The pressure difference, Δp, required for the solution of equation (III-12) is given by:

$$\Delta p = q_2 C_{pm}(1 - K_3) \qquad \text{(III-15)}$$

where q_2, C_{pm} and K_3 are functions of time. K_3 is defined and discussed later in this chapter.

From Figure 30, the semi-major diameter, b_d, of the drop is the arc length along the center line of the drop and is given by

$$(b_d)_i = .5\pi\, b_{i-1}\left(1 - \frac{\epsilon^2}{4} - \frac{3\epsilon^4}{64} - \frac{45\epsilon^6}{2304}\right) \qquad \text{(III-16)}$$

where

$$\epsilon^2 = 1 - \left\{b_{i-1} - (a_d)_i\right\}^2 / b_{i-1}^2$$

The mass of the drop at time, T, is given by

$$m_i = m_{i-1} + \Delta m_i \qquad \text{(III-17)}$$

where Δm_i is the mass loss from the drop as determined by a modified version of Taylor's[5] boundary layer stripping analysis which is developed in Appendix II. The mass loss, Δm_i, is given by

$$\Delta m_i = -(2\pi b_{i-1})^{3/2} K_4 \beta^{5/6} (1-\beta W_i)^{1/2} Z_2'^{1/2} R_\mu^{-1/3} \Delta T_i$$
$$-.065\pi b_{i-1} S_i (f_i + f_{i-1}) \Delta T_i \qquad \text{(III-18)}$$

The radius of the frontal surface of the drop is given by

$$b_i = \{(.75m/\pi a_d)_i\}^{1/2} \qquad \text{(III-19)}$$

Equations (III-14), (III-16), (III-17) and (III-19) define the mass and approximate shape of the drop. Since the shape of the drop is assumed to be fixed during the calculation interval, the acceleration of the center of gravity and the stagnation point of the drop is the same and is given by equation (AII-20). Hence, the velocity of the stagnation point, W_L, is readily found by equation (III-4) and the displacement, X_L, by equation (III-5).

Alternatively, as in the analysis of the experimental data, the velocity and displacement of the stagnation point can be found by considering a cylindrical element of mass which contains the stagnation point.

The force acting on the cylindrical element is given by (see Figure 8)

$$F = 2\pi y^2 \Delta p \qquad \text{(III-20)}$$

The mass of the element is

$$m = 4\pi y^2 a_d \qquad \text{(III-21)}$$

By Newton's Second Law the acceleration of the element is

$$\alpha = .5 \Delta p / a_d \qquad \text{(III-22)}$$

The velocity of the stagnation point, W_L, is now readily found by equation (III-4) and the displacement, X_L, by equation (III-5).

The pressure difference, Δp, in equation (III-22) is the difference of the pressures acting on the upstream and downstream sides of the drop. The pressure on the upstream side of an axisymmetric ellipsoidal drop is given by

$$P_\ell = P_\infty + q_2 C_{pm}\left(1 - \frac{K_1 a^2 \sin^2\phi}{a^2 \sin^2\phi + b^2 \cos^2\phi}\right) \qquad \text{(III-23)}$$

where it has been assumed that the local pressure on the ellipsoid is the same as that found on a sphere by applying a tangent cone of constant vertex angle to both the ellipsoid

and the sphere. The local pressure on the downstream side of the drop is given by

$$p_\ell = p_\infty + q_2 C_{pm} K_3 \qquad \text{(III-24)}$$

K_1 and K_3 are parameters which occur if the relationships for pressure distribution on the upstream and downstream sides of a sphere considering both subsonic and supersonic flow are written, respectively, in the general forms

$$C_p = C_{pm}(1 - K_1 \sin^2\phi) \quad , \qquad \text{(III-24a)}$$

and

$$C_p = C_{pm} K_3 \qquad \text{(III-24b)}$$

K_1 for supersonic flow is unity,[13] and for subsonic incompressible flow[1] $K_1 = 2$. On the rearward side of the drop the pressure is taken to be constant and independent of ϕ. For supersonic flow $K_3 = 0$, and for subsonic incompressible flow $K_3 = -.5$. Transonic flow is assumed to occur between $M_R = 0.7$ and $M_R = 1.3$. In this regime a linear transition from the subsonic incompressible to the supersonic values of K_1 and K_3 is assumed; K_1 and K_3 are thus given by

$$K_1 = 1.5 - \left\{\frac{|M_R - .7| - |M_R - 1.3|}{1.2}\right\}$$

$$K_3 = -.25 + \left\{\frac{|M_R - .7| - |M_R - 1.3|}{2.4}\right\}$$

where M_R is the Mach number of the air stream relative to the drop.

The equations for deformation and fragmentation of the drop are solved by a forward marching numerical technique employing a time interval sufficiently small that negligible error is introduced in any given time interval by assuming time dependent variables are constant during that time interval.

Theoretical results and experimental data are compared in the next chapter.

CHAPTER IV

DISCUSSION OF RESULTS

The numerical solutions for displacement of the drop indicate that for the conditions of this study the maximum time for the shock wave to pass over the drop is 1.375 μseconds or a dimensionless time of .0505. The displacement of the drop during this time period is .009 body diameters, which is not measurable on photographs. The major axis is calculated to have changed less than .0003 percent. Thus the assumption made herein that the drop remains spherical during this period is justified, and the observations of Engel[1] and of Ranger and Nicholls that the drop exhibits no measurable displacement or distortion during shock passage are confirmed.

For the analysis of the deformation and fragmentation of the water drop a relatively simple analytical model was sought which would approximate the observed displacement of the stagnation point of the drop, show a variation of the semi-major diameter of the frontal surface of the drop similar to that observed in the experimental results and show a change in mass of the drop approximately the same as that found from the experimental data. In addition, the analytical model should reasonably determine the velocity of the stagnation point of the drop and the semi-minor and semi-major axes or the eccentricity of the drop.

The theoretical model employed in the analysis is based on the assumptions of potential flow within the drop and mass flow from the drop by the stripping of a viscous surface layer of liquid at the equator of the drop which is taken to coincide with a point 90 degrees from the stagnation point

on the spherical frontal surface of the drop.

Calculated results of the theory are shown for the cases of shock wave Mach numbers, M_s, of 1.6 and 3.0 which cover the range of the experimental data of this study.

The assumption of potential flow within the drop eliminates viscous flow considerations from the distortion and accounts for mass continuity during distortion of the drop analysis. While this assumption appears to be desirable in this first attempt to model simultaneously drop deformation and fragmentation, it is seen by comparison of analytical and experimental results for the semi-minor diameter, a_d, shown in Figures 31 and 12, respectively, that the model semi-minor diameter does not decrease initially as rapidly as observed in experiment. This indicates that the assumed velocity potential for the liquid flow within the drop is inexact. As will be seen, however, this simple potential is quite adequate for the principal purpose of the theory, that is, the prediction of the mass history of the drop.

Since the major diameter, B, of the frontal surface of the drop is directly related to the semi-minor diameter as is shown by equation (III-19) for mass of the drop, it is expected that the analytically determined major diameter, B, will exhibit a less rapid initial increase than that observed for B in the experimental data. Comparison of Figures 10 and 32 show this to be the case. This comparison also indicates that the maximum analytically determined values of the major diameter, B, are within 10 percent of the maximum experimentally measured values. Further, the dimensionless time at which the calculated major diameter, B, reaches a maximum is within 15 percent of the experimentally observed time at which B reaches a maximum. The differences between experimentally observed and theoretical values of a_d and B during

latter phases of fragmentation of the drop are attributed to assumptions made in the boundary layer stripping analysis and are discussed later in this chapter.

Figure 33 presents the calculated mass of the drop normalized to the initial mass of the drop. Comparison of this figure with Figure 28 for the experimentally determined normalized mass of the drop indicates good agreement between the observed and calculated values. From these figures it is also seen that the calculated mass of the drop is somewhat less than the experimentally observed value when the mass of the drop is reduced to approximately 20 percent of its original mass. From Figure 31 it is seen that at approximately $T = 1.7$ the drop is becoming very thin and clearly the viscous boundary layer is no longer small compared to the thickness of the drop. Hence the theoretical model which is based on the assumption of a thin boundary layer is inaccurate. This deterioration of the model for mass loss is also reflected through equation (III-19) in the behavior of the major diameter of the frontal surface as shown in Figure 32 for $T > 1.8$ to 2.0. Similarly, the semi-minor diameter, a_d, is also affected through equations (III-16) and (III-12).

Figure 34 presents the theoretical displacement of the stagnation point of the drop. Comparison of Figure 34 and 11 indicates that the theoretical model predicts smaller displacements during the breakup process than are observed experimentally. At $T = 2.5$, however, the experimentally observed displacement falls between the calculated values for the range of shock wave Mach number of this study. The difference between the experimentally observed and the calculated displacement is attributed primarily to the assumption made in the analysis that the maximum pressure coefficient varies linearly with the relative Mach number, M_R, in

the transonic regime and is constant in the subsonic and supersonic regimes as given by equation (III-6).

This or a similar assumption as to the variation of the local pressure coefficient, C_p, on a sphere was necessary since no experimental data on pressure distributions around spheres or hemispheres in the transonic regime appear to be available.

Figure 35 presents the theoretical velocity of the stagnation point of the drop. Since the velocity is the time rate of change of the displacement, it is to be expected from the slope of the displacement curves in Figure 34 that the predicted velocity will be larger than that experimentally observed. Comparison of Figures 27 and 35 show this to be the case with the calculated velocity being approximately 25 percent greater than the experimentally determined velocity at $T = 2.5$. This difference is also attributed to the assumed linear variation of the maximum pressure coefficient as discussed in the preceding paragraph.

Figure 36 presents the calculated time variation of the eccentricity of the drop. Comparison of this figure with Figure 14 indicates similar timewise variation of the eccentricity. While both the theoretically predicted and experimentally determined eccentricities approach unity between $T = .6$ and $T = .7$, the experimentally determined value increases more rapidly than does the analytically predicted value. This is due to the relatively slower decrease in the analytically predicted variation in the semi-minor diameter, a_d, of the drop than is observed in the experimental results as was discussed earlier in this chapter.

CHAPTER V

CONCLUSIONS

This investigation of deformation and fragmentation of a water drop due to shock wave impact has produced several new findings from both the experimental and theoretical results.

The primary experimental data which are measurements of the displacement and the major diameter of the deformed water drop are in good agreement with those of other investigators.

Analysis of the experimental data shows that the water drop is deformed into an axisymmetric shape which has a nearly spherical ellipsoidal frontal, or windward, surface and a concaved rear surface.

Determination of the mass of the drops as a function of time from the experimental data permits a new criterion to be used to establish the time for complete fragmentation or breakup of the drop. Using the time at which the mass of the drop is reduced to approximately 1 percent of its original mass, it is found that drop breakup occurs at approximately $T = 2.5$. This is approximately one-half of the time identified by other investigators who used the criterion that breakup time is that at which the water drop is observed to be reduced to a trace of mist on photographs of water drop fragmentation. Using this criterion the time for complete breakup of the water is typically given as $T = 5.0$.

The approximate analytical model developed in this study indicates simultaneous deformation and mass loss from a water drop can be treated using a simple theoretical model.

It is concluded from a comparison of theory and experiment that the classical Taylor's boundary layer stripping analysis must be modified in order to obtain a realistic prediction of the mass history of the water drop. The modification proposed herein (Appendix II) permits the viscous profile to extend through the entire drop as it becomes thin.

It is further concluded that while the assumption of potential flow within the drop is satisfactory for an approximate theoretical model as was used herein, a more exact theory of the internal flow should be developed.

It is also concluded that the general lack of experimental data on the pressure distributions on spheres, hemispheres and ellipsoids in the transonic and low supersonic flow regime will restrict the accuracy of calculations on the displacement, deformation and fragmentation of water drop which are imparted with shock waves moving in the Mach number range of approximately 1.6 to 4.0.

Finally it is concluded from the good agreement between the experimentally and theoretically determined mass of the drop that the mass calculation is relatively insensitive to the precise form of the potential flow function used to calculate deformation of the drop.

FIGURE 1. EXPERIMENTAL ARRANGEMENT

FIGURE 2. WATER DROP INJECTORS

FIGURE 3. TEST SECTION

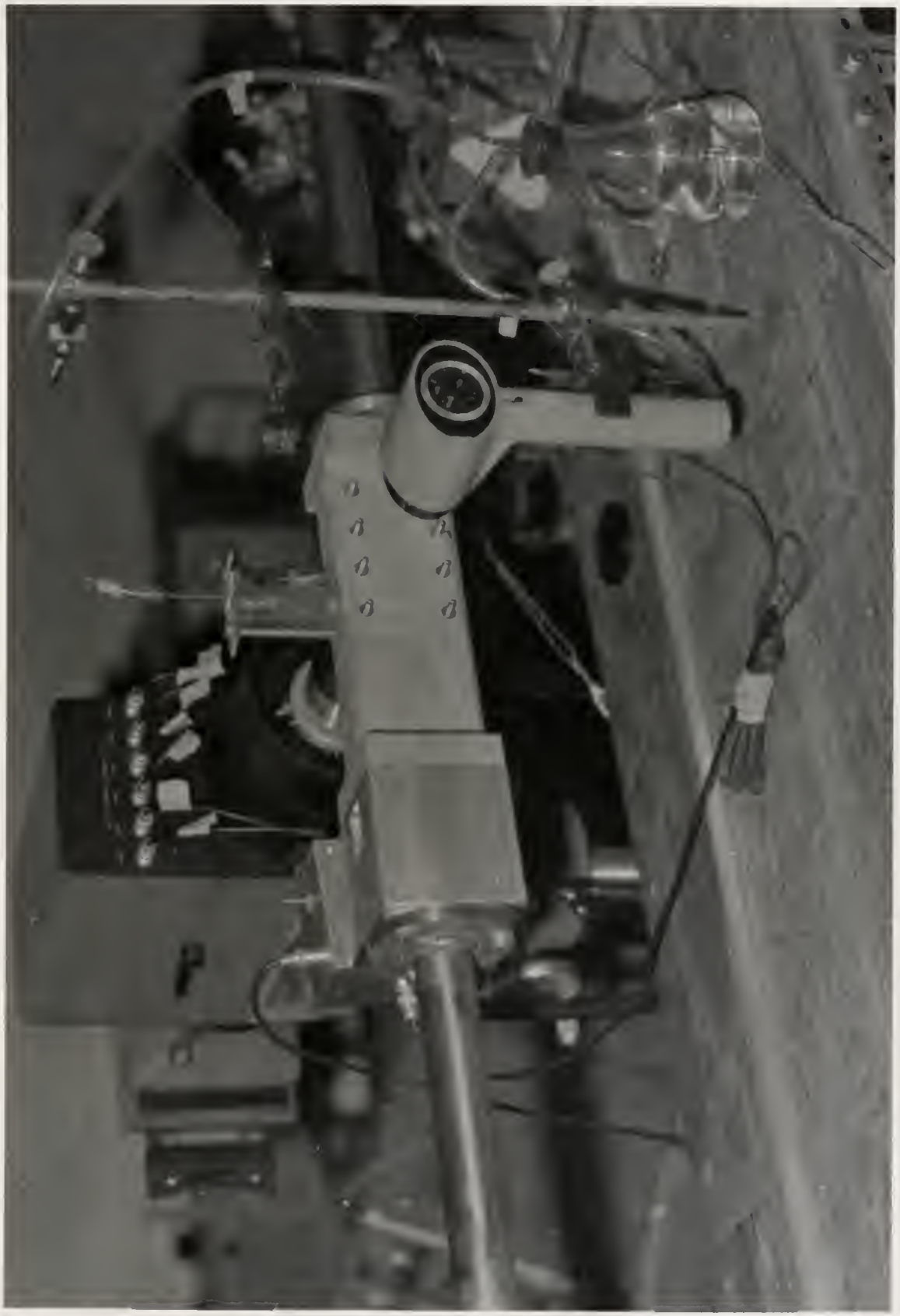

FIGURE 4. BACK LIGHTING ARRANGEMENT

a. b. c.

FIGURE 5. TYPICAL SHADOW PHOTOGRAPH SEQUENCES: a. D=2.06 mm, M_s=1.84; b. D-2.74 mm, M_s=2.01; c. D=.985 mm, M_s=1.90

TABLE I
TIME SEQUENCE FOR PHOTOGRAPHS SHOWN IN FIGURE 5

	Dimensionless Time, T	Real Time, t, μ seconds
Figure 5a - Exposure; D = 2.06 mm.		
1	0	0
2	.460	44
3	.985	94
4	1.140	109
5	1.455	139
Figure 5b - Exposure; D = 2.74 mm.		
1	0	0
2	.220	30
3	1.155	124
4	2.060	224
5	2.980	324
Figure 5c - Exposure; D = .985 mm.		
1	0	0
2	1.200	55
3	1.850	85
4	2.740	125
5	4.260	195

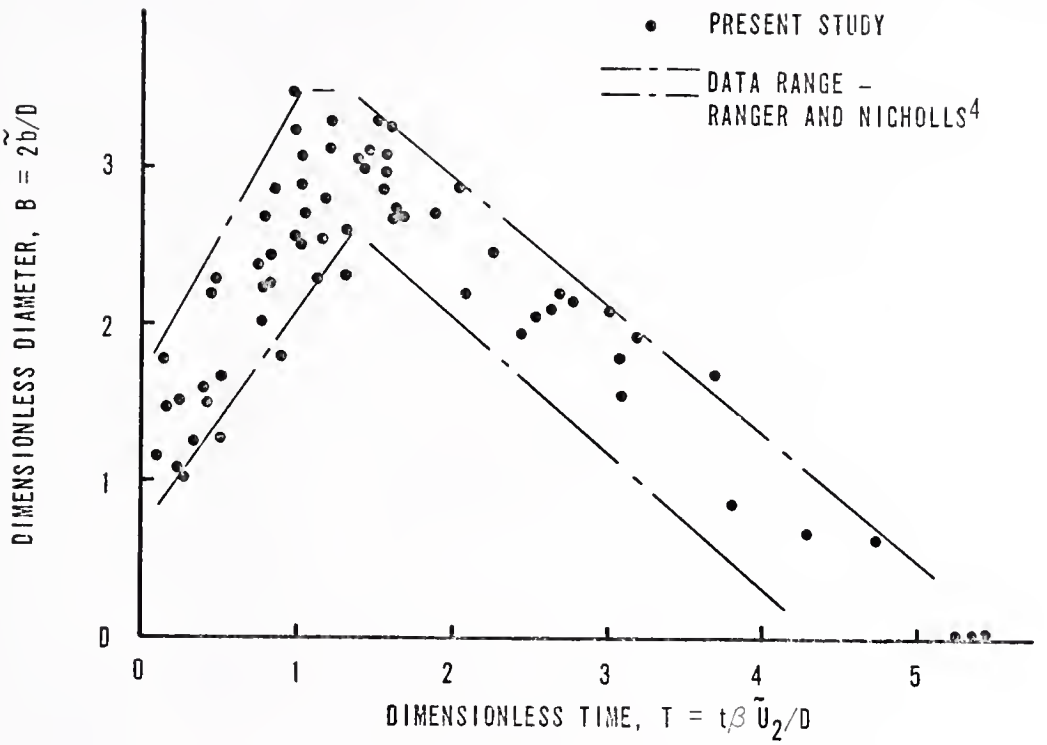

FIGURE 6. EXPERIMENTAL DROP DEFORMATION DATA

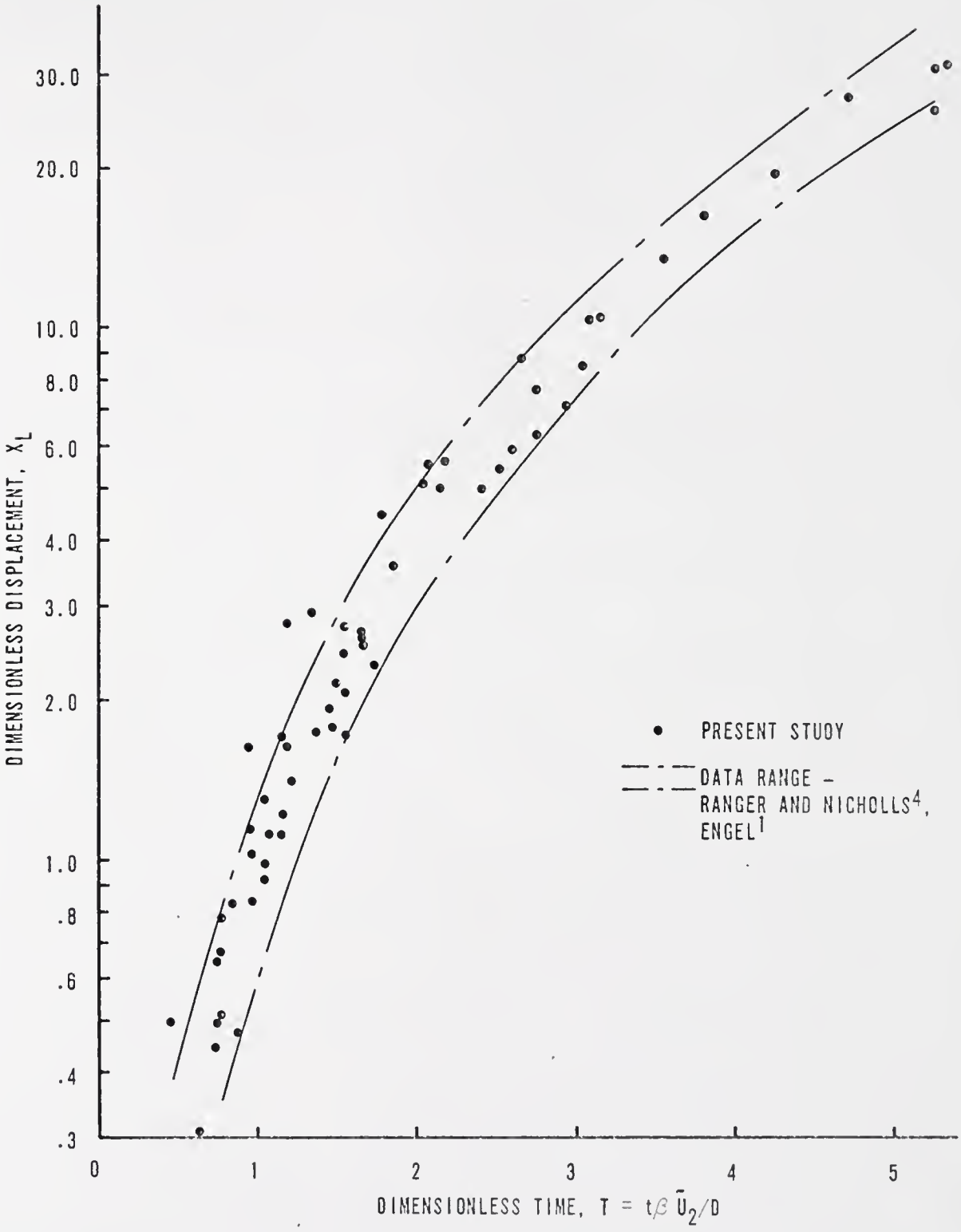

FIGURE 7. EXPERIMENTAL DROP STAGNATION POINT DISPLACEMENT DATA

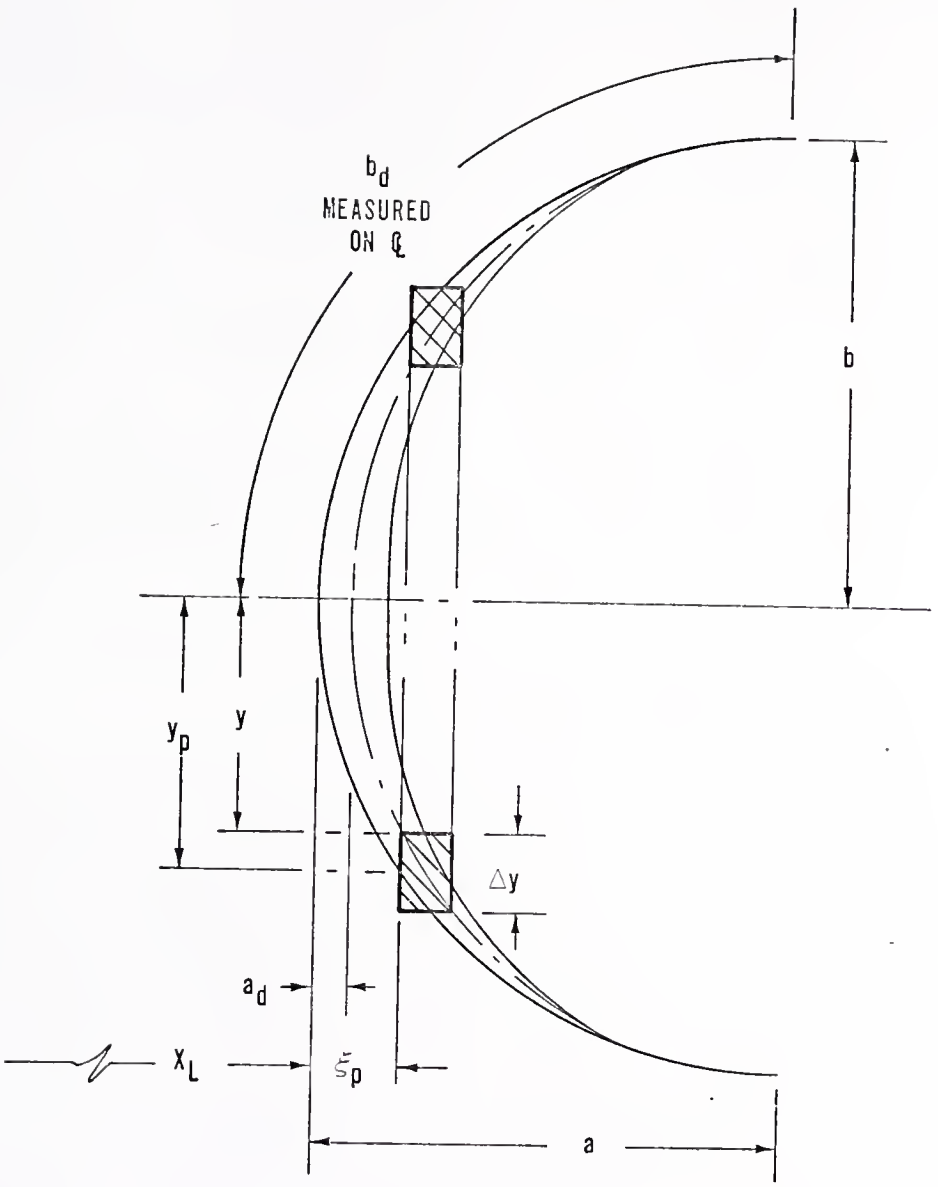

FIGURE 8. COORDINATE SYSTEMS FOR ANALYSIS OF EXPERIMENTAL DATA

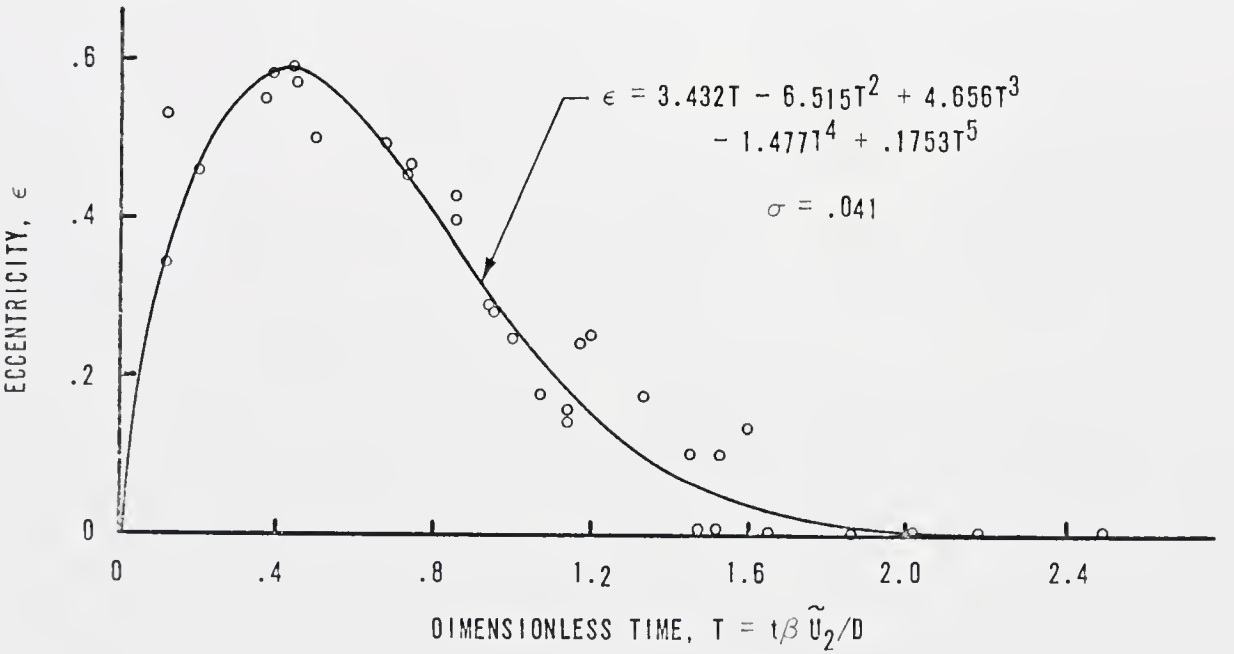

FIGURE 9. MEASURED ECCENTRICITY OF THE FRONTAL SURFACE OF THE DROP AND LEAST MEAN SQUARE CURVE FIT TO THE DATA

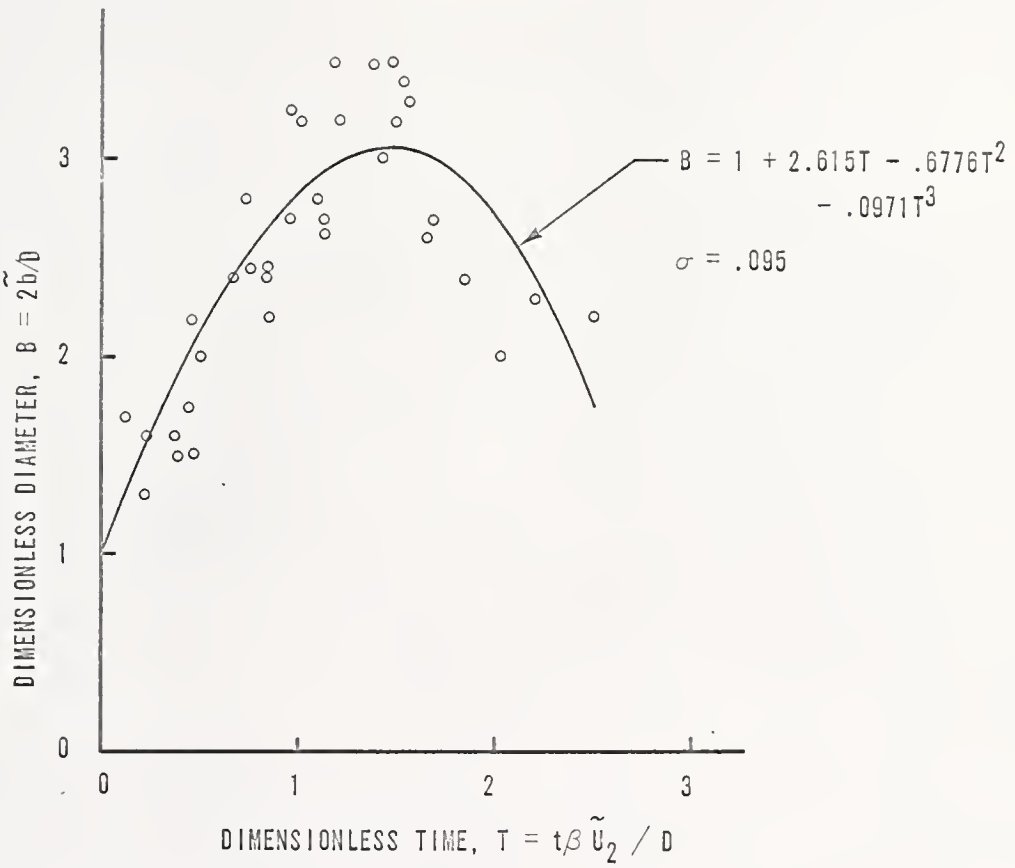

FIGURE 10. MEASURED DEFORMATION OF THE DROP AND LEAST MEAN SQUARE CURVE FIT TO THE DATA

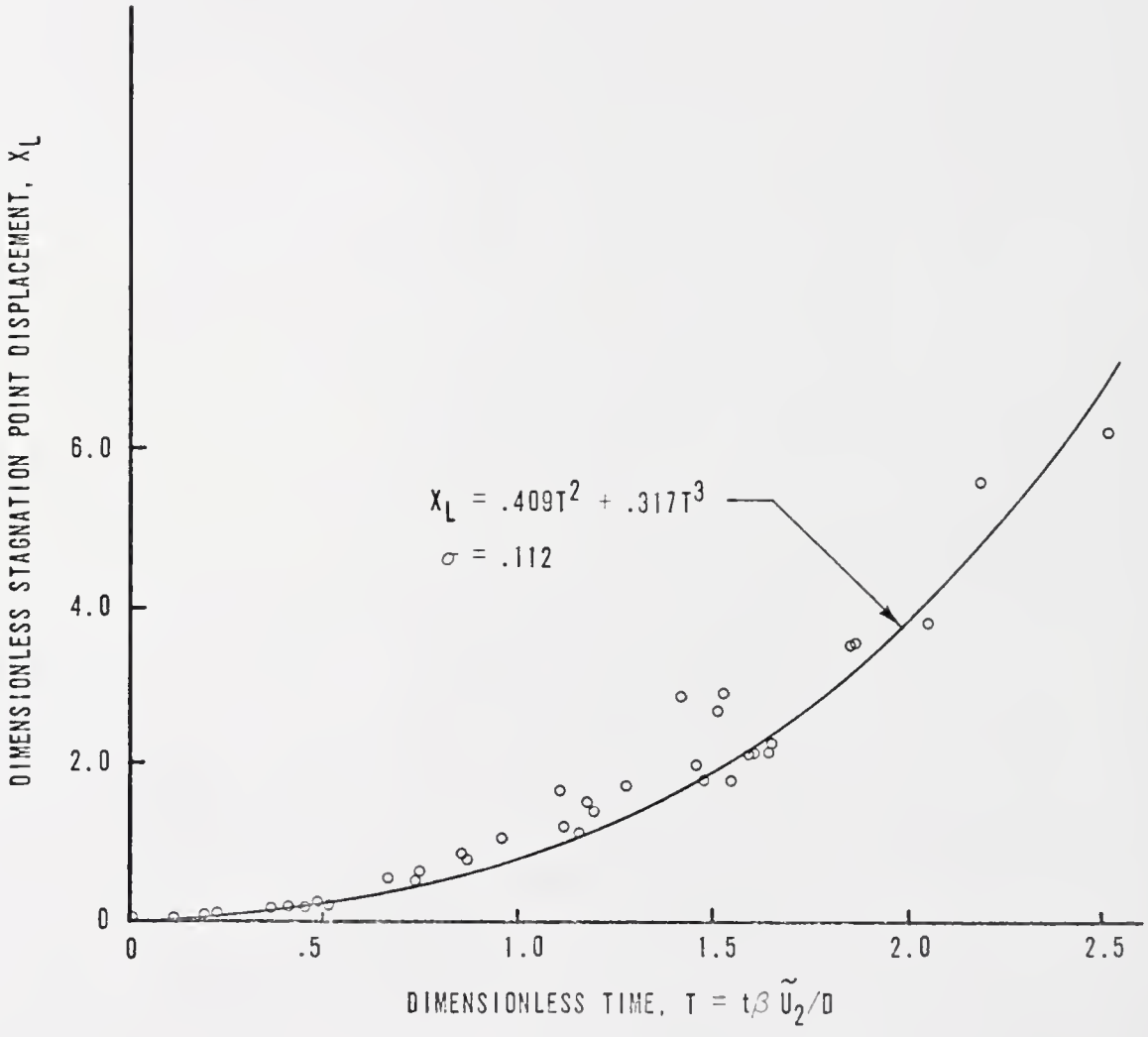

FIGURE 11. MEASURED DISPLACEMENT OF THE STAGNATION POINT OF THE DROP AND LEAST MEAN SQUARE CURVE FIT TO THE DATA

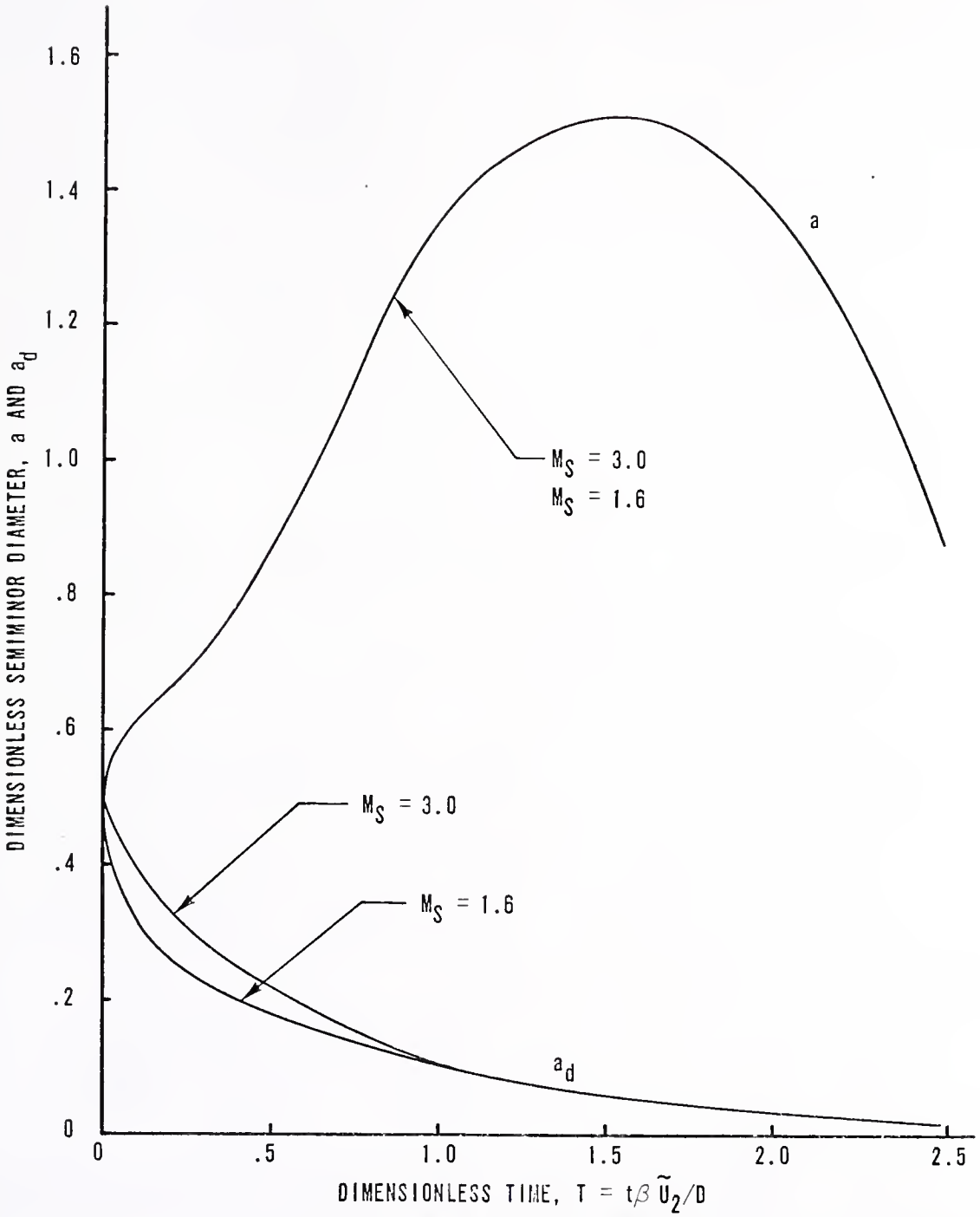

FIGURE 12. MEASURED SEMI-MINOR DIAMETERS OF THE FRONTAL SURFACE OF THE DROP AND OF THE DROP

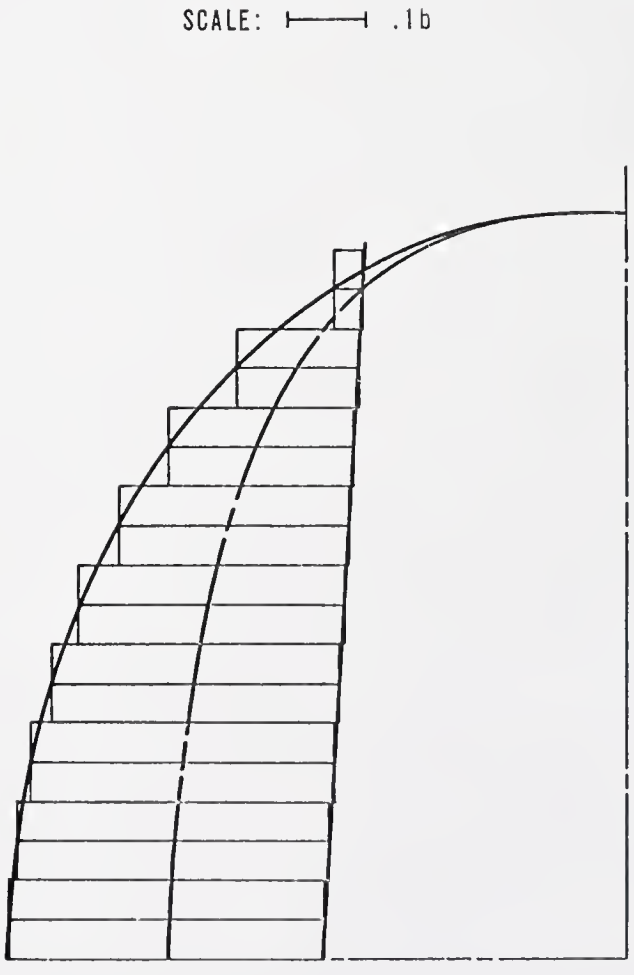

FIGURE 13. MEASURED CROSS SECTIONAL SHAPE OF THE FRONTAL SURFACE AND CALCULATED CROSS SECTIONAL SHAPE OF THE DROP AT T = .4

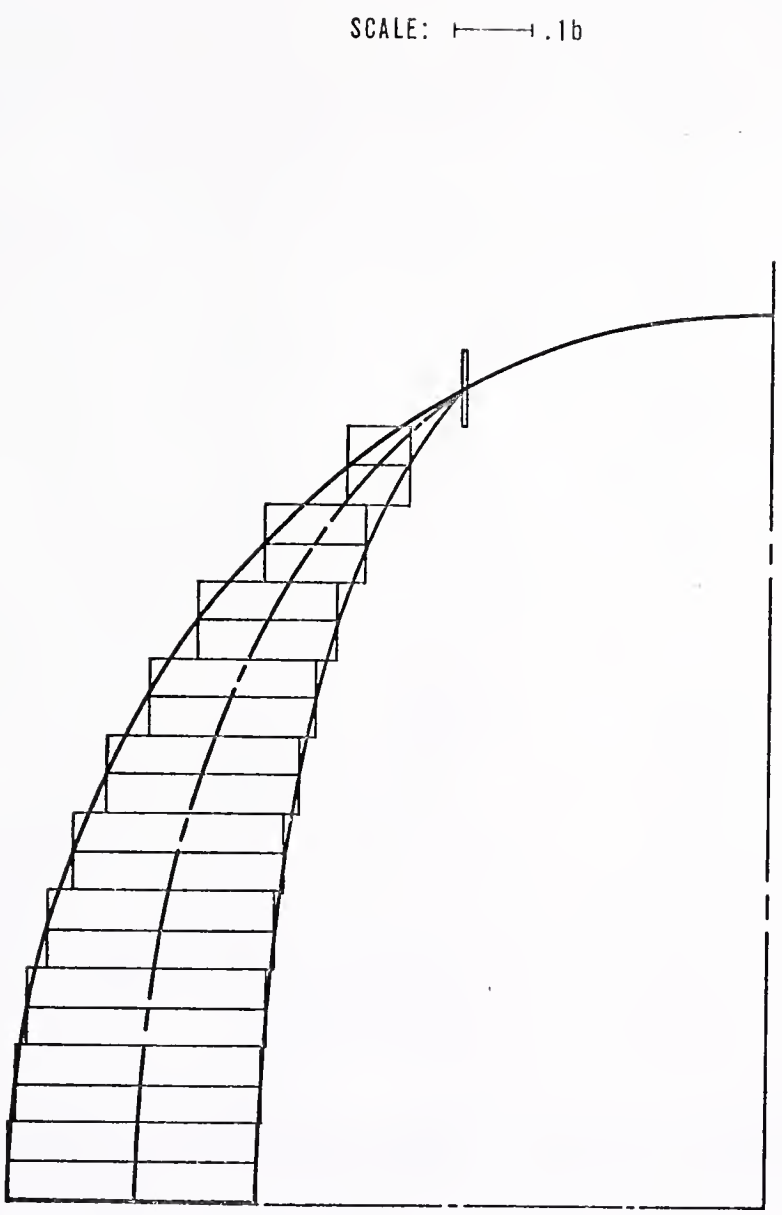

FIGURE 14. MEASURED CROSS SECTIONAL SHAPE OF THE FRONTAL SURFACE AND CALCULATED CROSS SECTIONAL SHAPE OF THE DROP AT T = .6

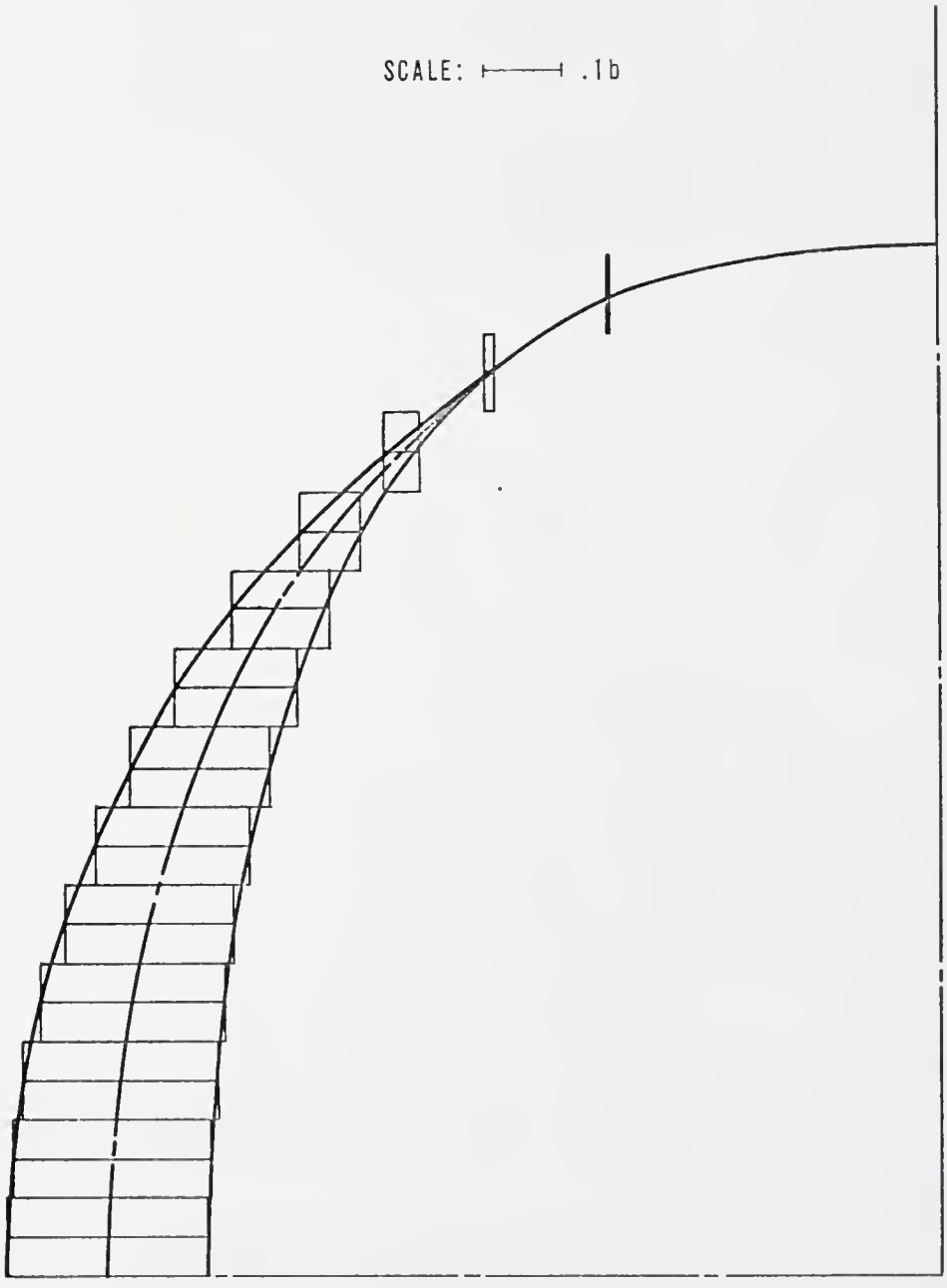

FIGURE 15. MEASURED CROSS SECTIONAL SHAPE OF THE FRONTAL SURFACE AND CALCULATED CROSS SECTIONAL SHAPE OF THE DROP AT T = .8

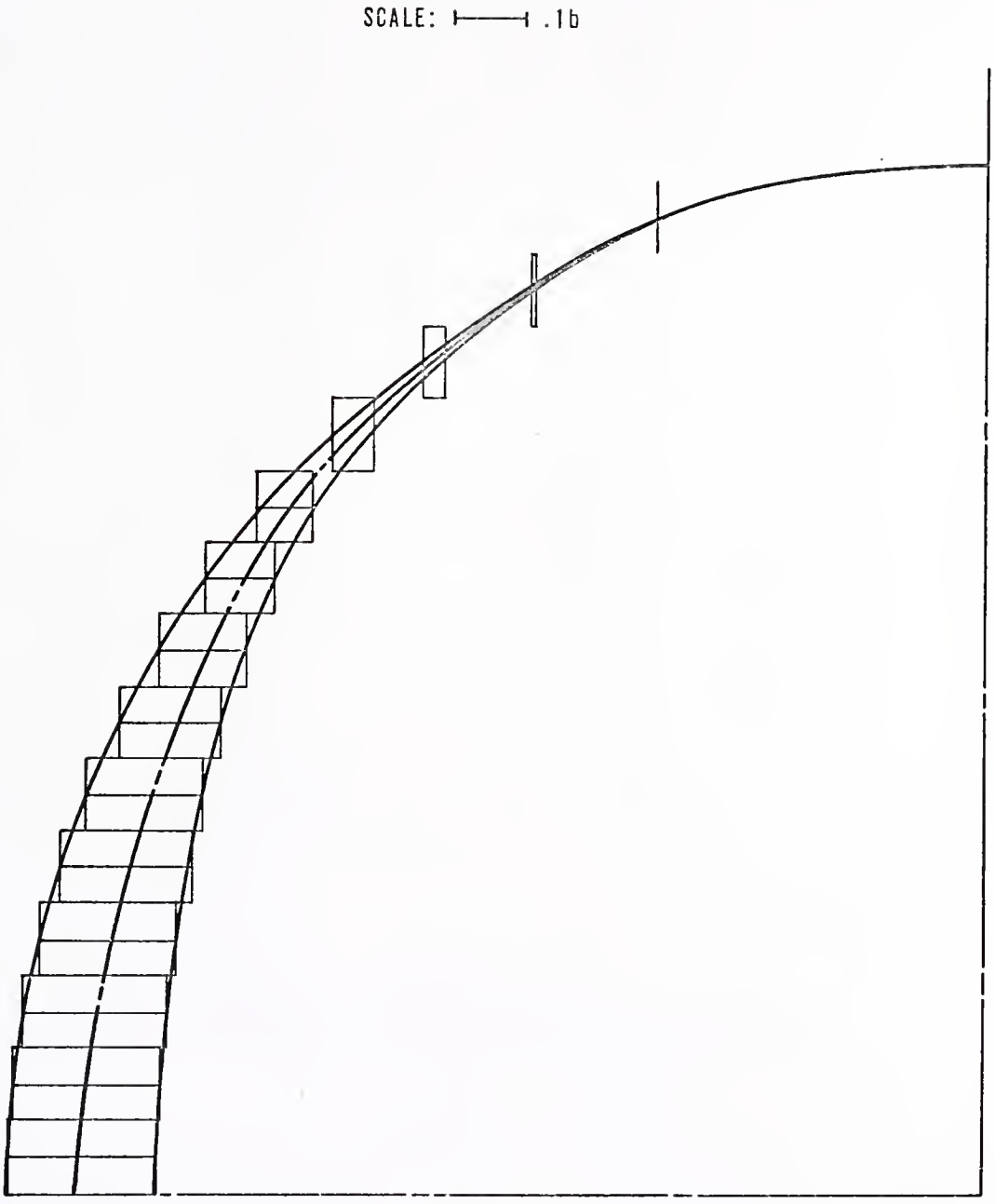

FIGURE 16. MEASURED CROSS SECTIONAL SHAPE OF THE FRONTAL SURFACE AND CALCULATED CROSS SECTIONAL SHAPE OF THE DROP AT T = 1.0

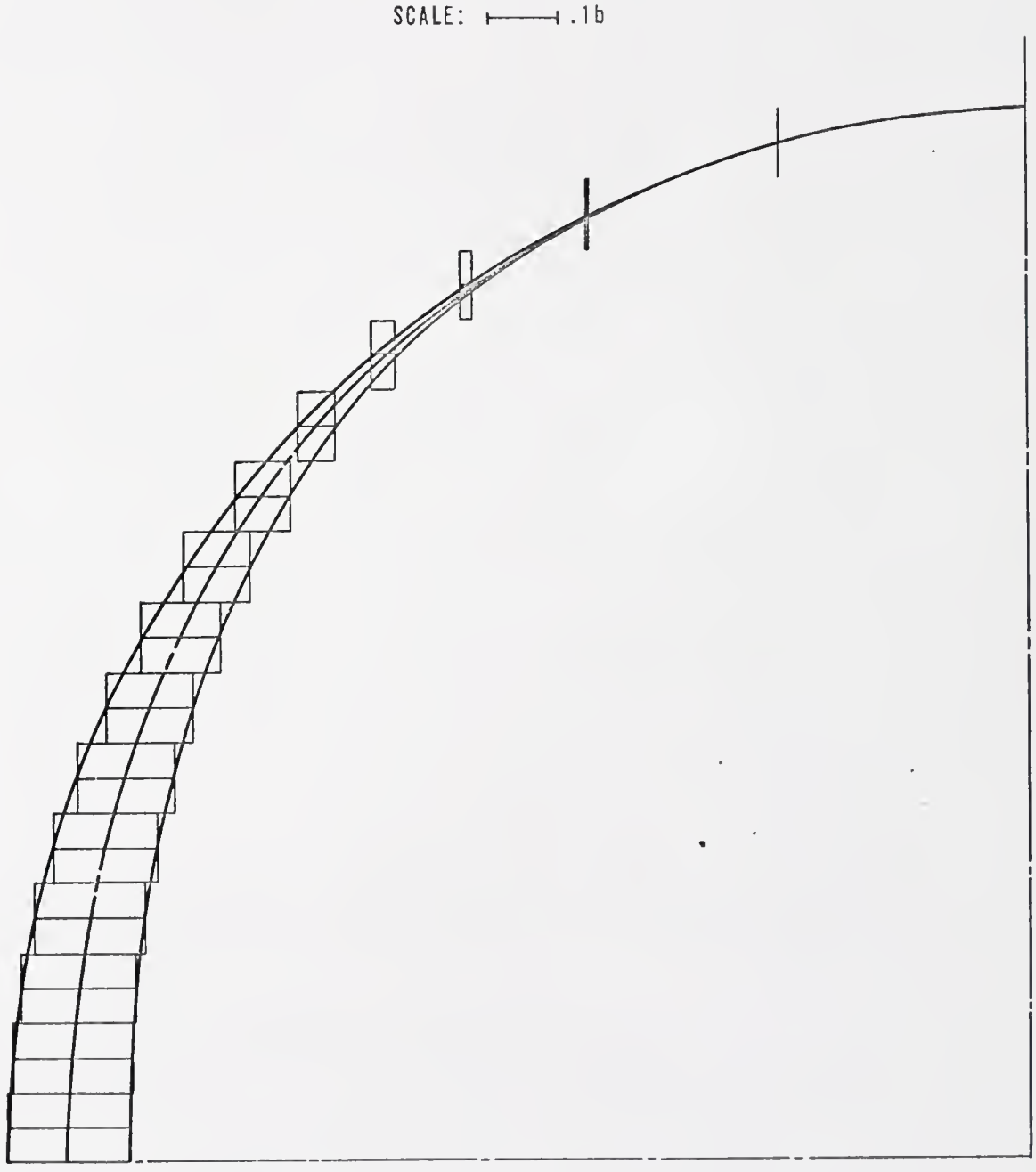

FIGURE 17. MEASURED CROSS SECTIONAL SHAPE OF THE FRONTAL SURFACE AND CALCULATED CROSS SECTIONAL SHAPE OF THE DROP AT T = 1.2

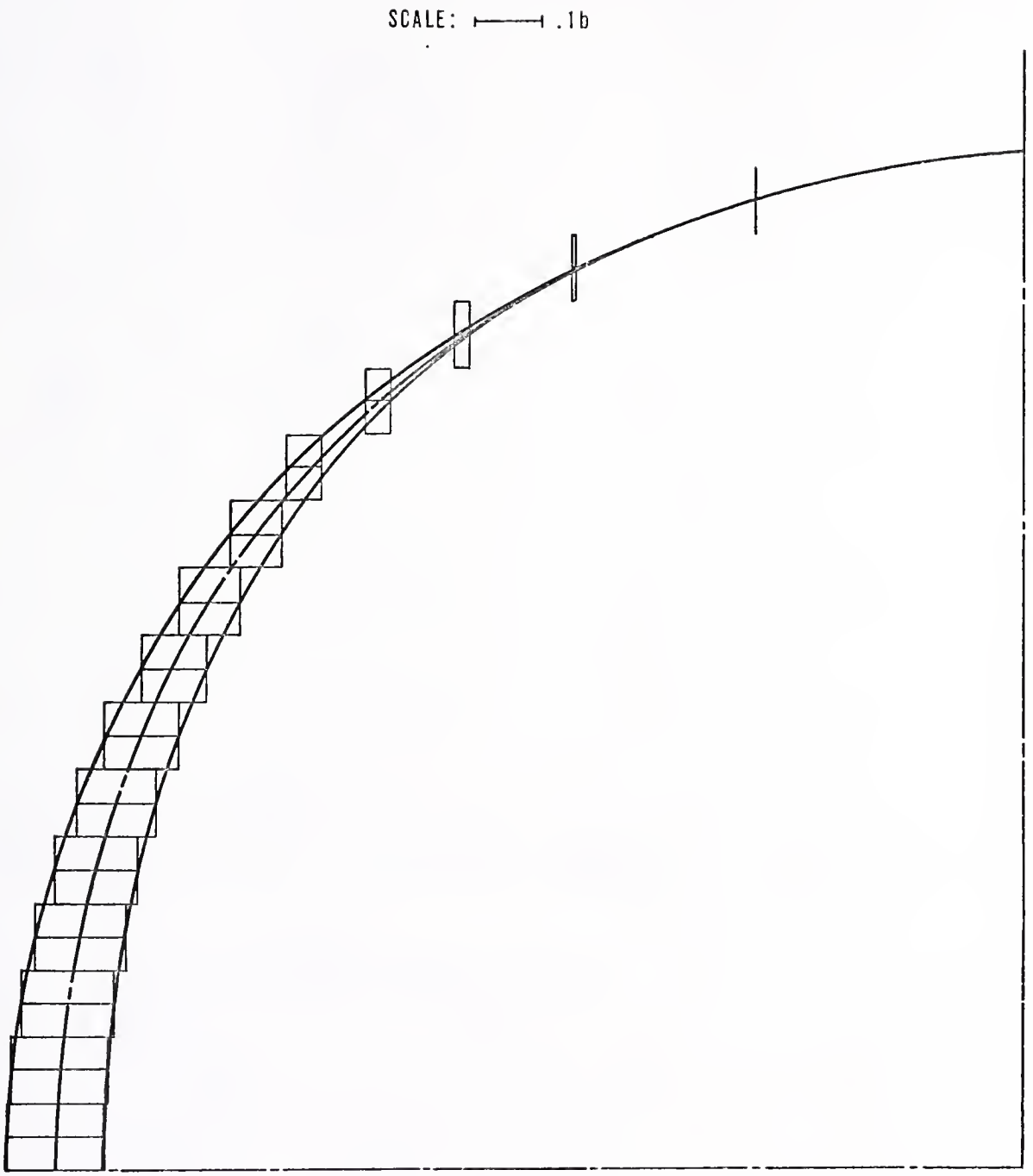

FIGURE 18. MEASURED CROSS SECTIONAL SHAPE OF THE FRONTAL SURFACE AND CALCULATED CROSS SECTIONAL SHAPE OF THE DROP AT T = 1.4

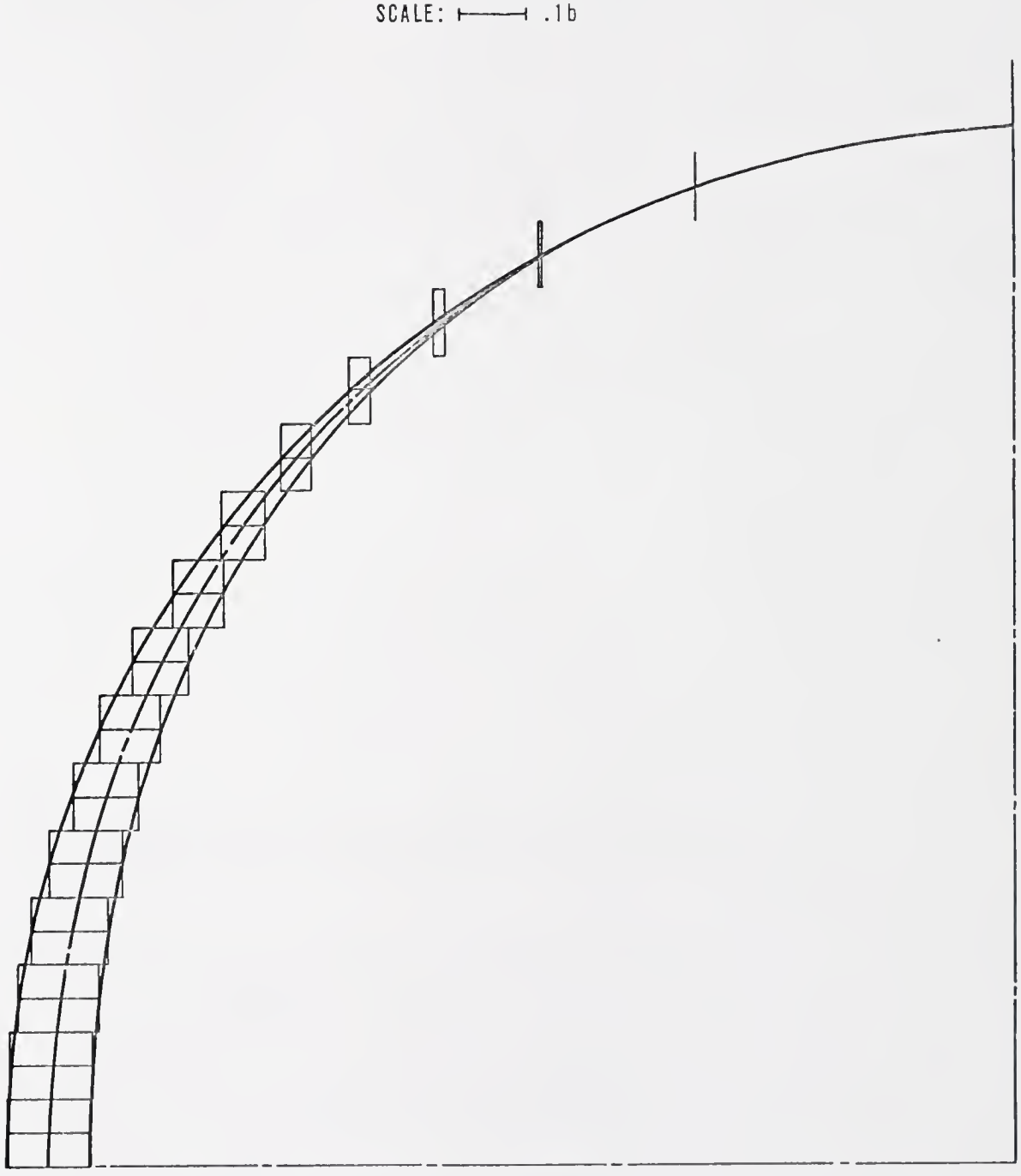

FIGURE 19. MEASURED CROSS SECTIONAL SHAPE OF THE FRONTAL SURFACE AND CALCULATED CROSS SECTIONAL SHAPE OF THE DROP AT T = 1.6

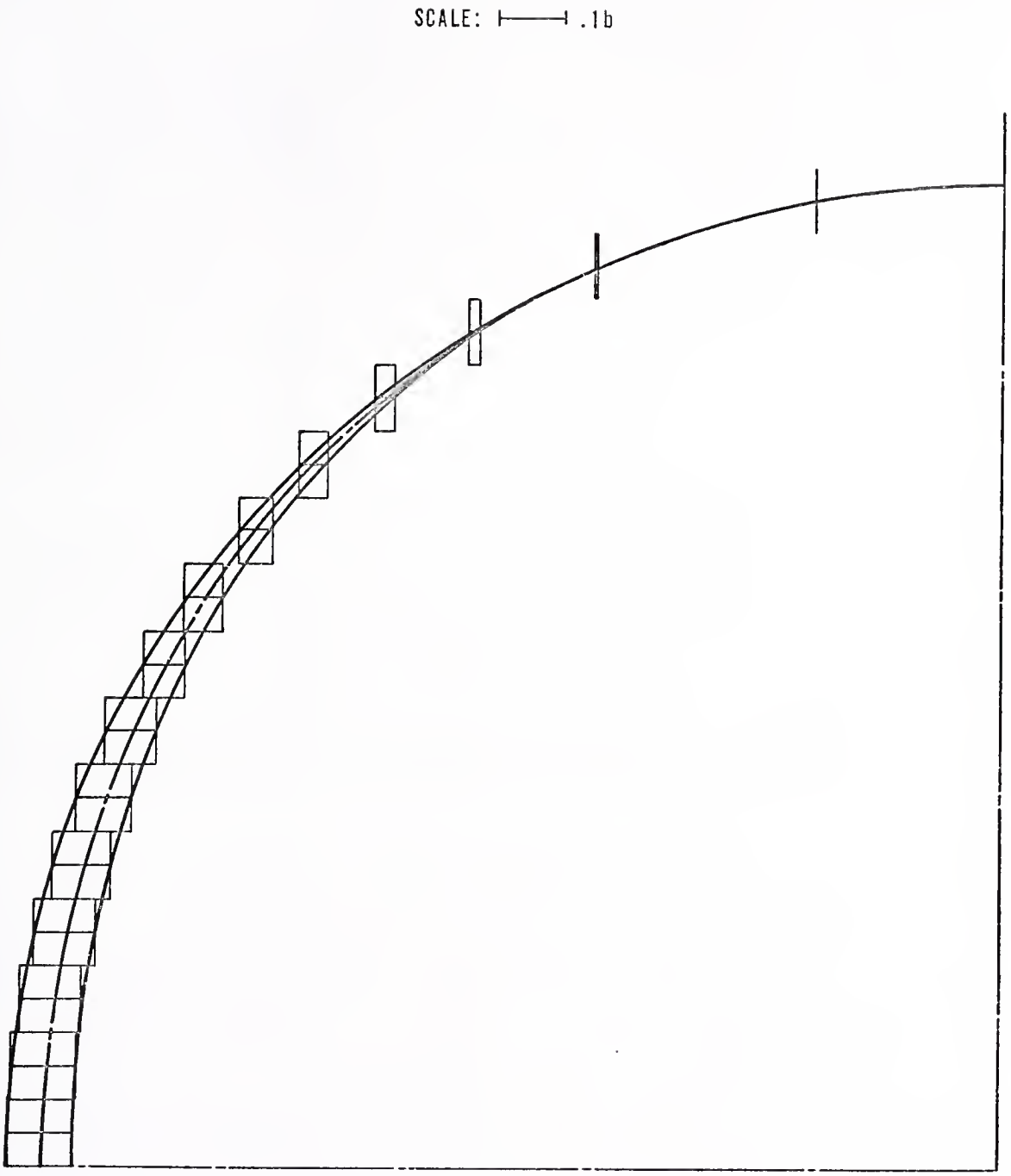

FIGURE 20. MEASURED CROSS SECTIONAL SHAPE OF THE FRONTAL SURFACE AND CALCULATED CROSS SECTIONAL SHAPE OF THE DROP AT T = 1.8

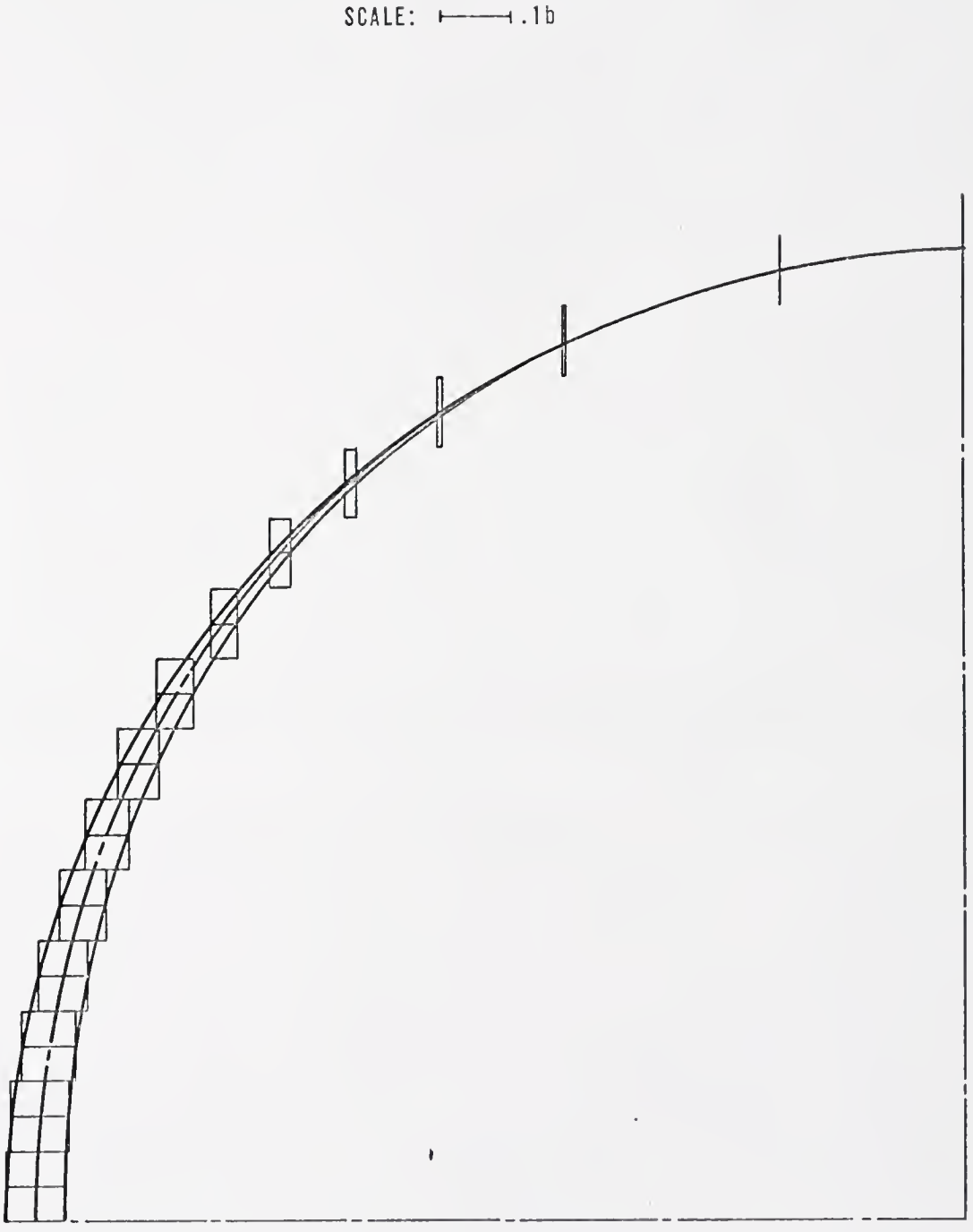

FIGURE 21. MEASURED CROSS SECTIONAL SHAPE OF THE FRONTAL SURFACE AND CALCULATED CROSS SECTIONAL SHAPE OF THE DROP AT T = 2.0

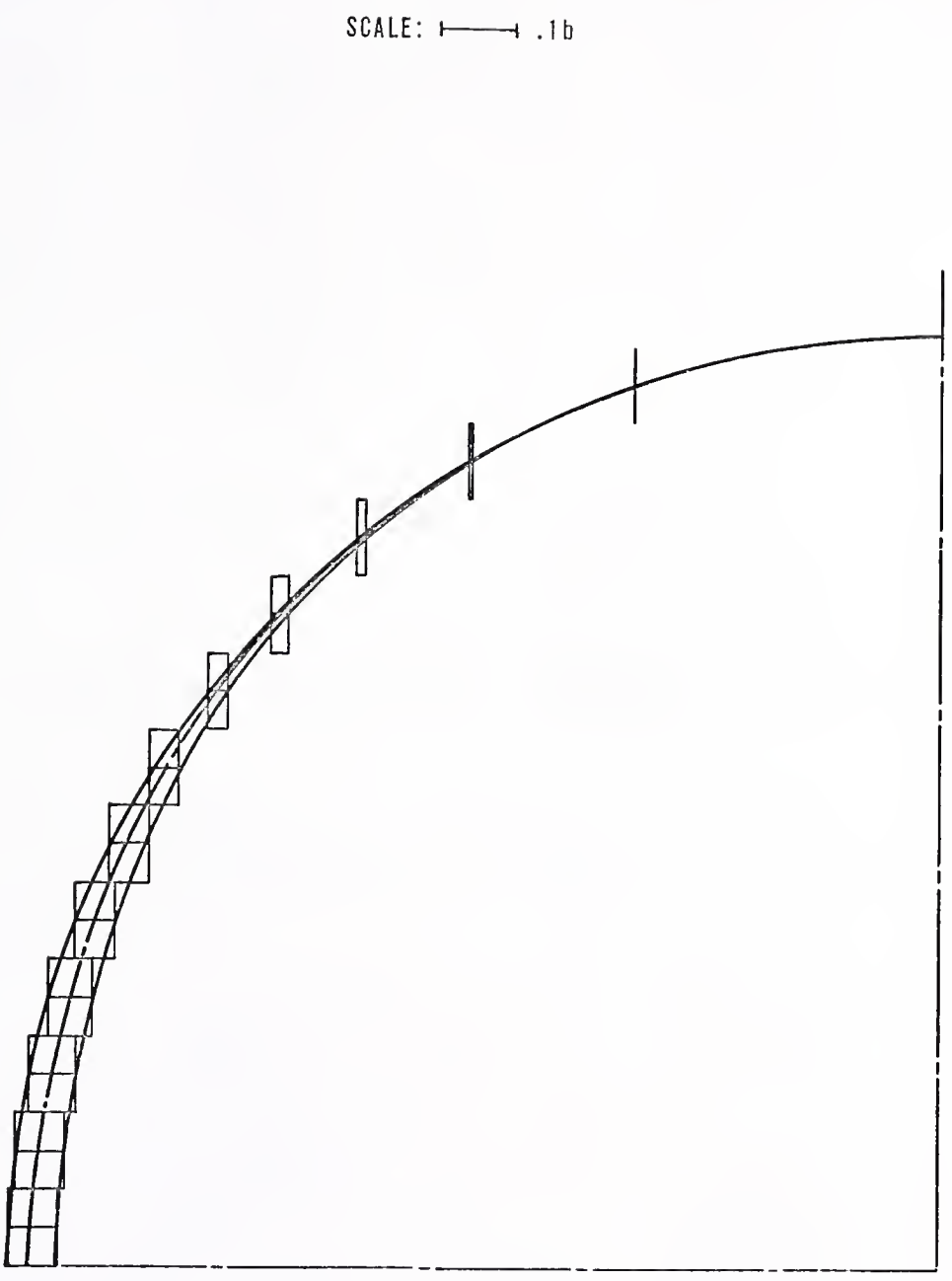

FIGURE 22. MEASURED CROSS SECTIONAL SHAPE OF THE FRONTAL SURFACE AND CALCULATED CROSS SECTIONAL SHAPE OF THE DROP AT T = 2.2

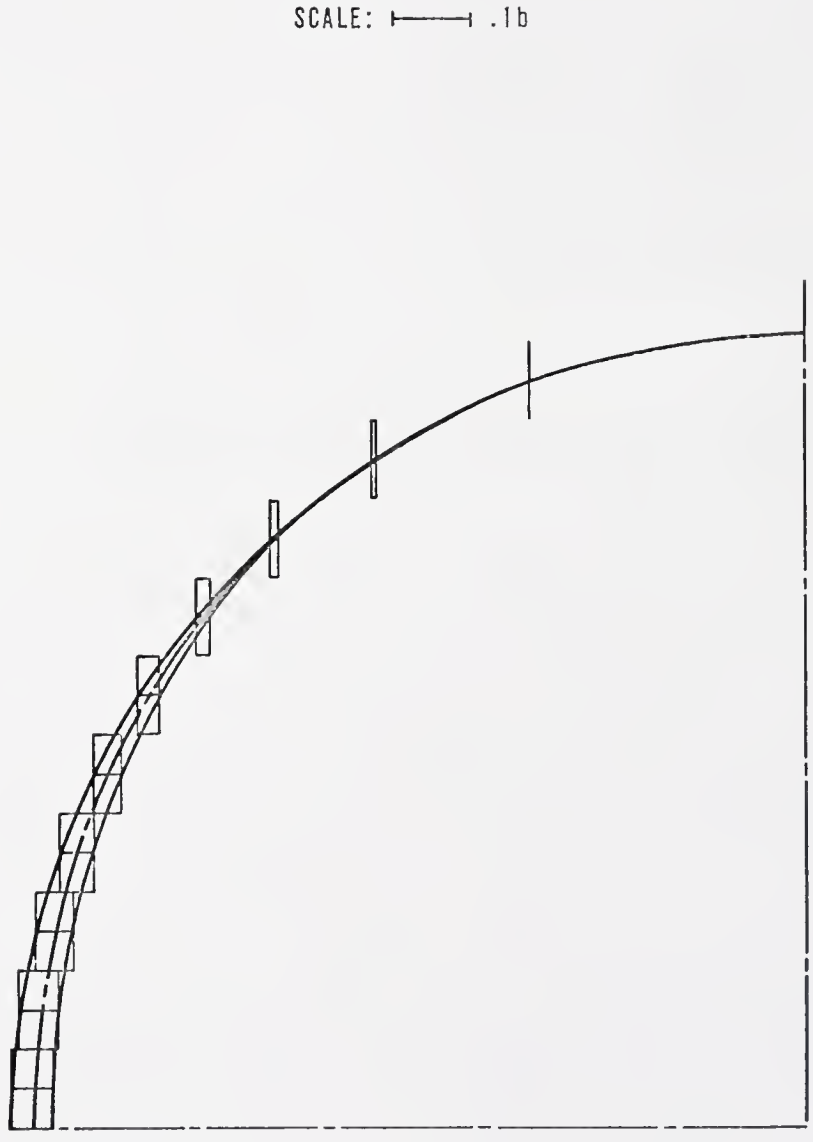

FIGURE 23. MEASURED CROSS SECTIONAL SHAPE OF THE FRONTAL SURFACE AND CALCULATED CROSS SECTIONAL SHAPE OF THE DROP AT T = 2.4

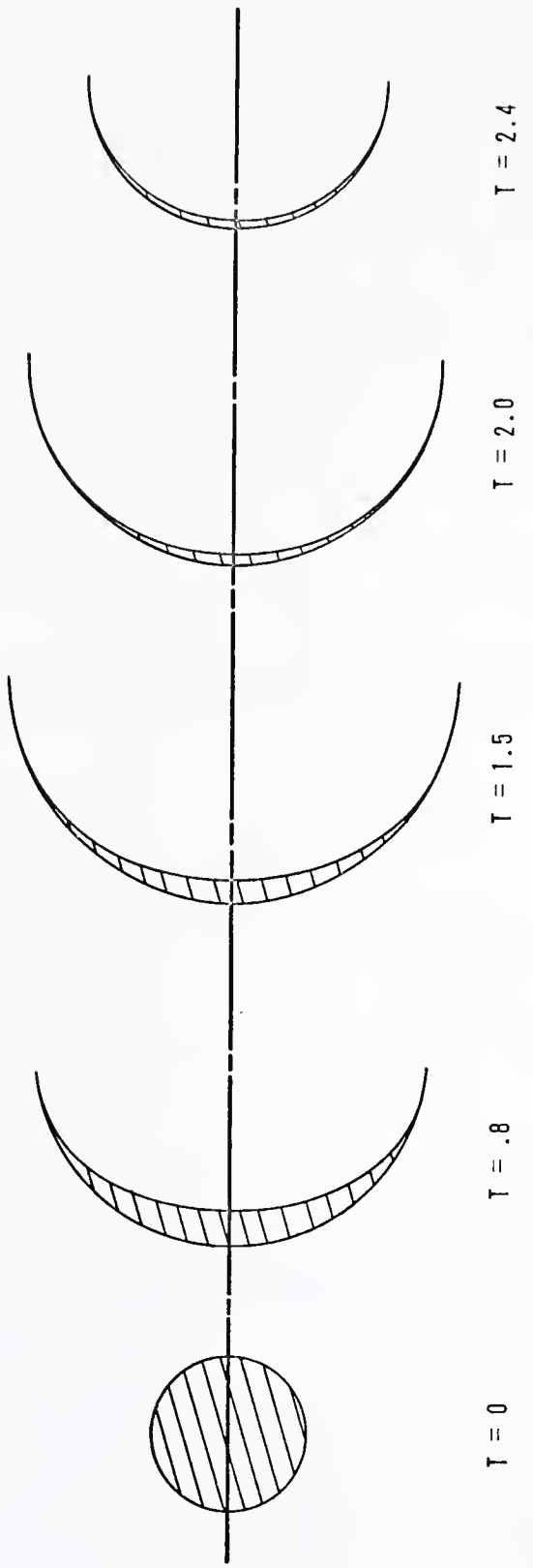

FIGURE 24. SUMMARY OF FIGURES 13-23

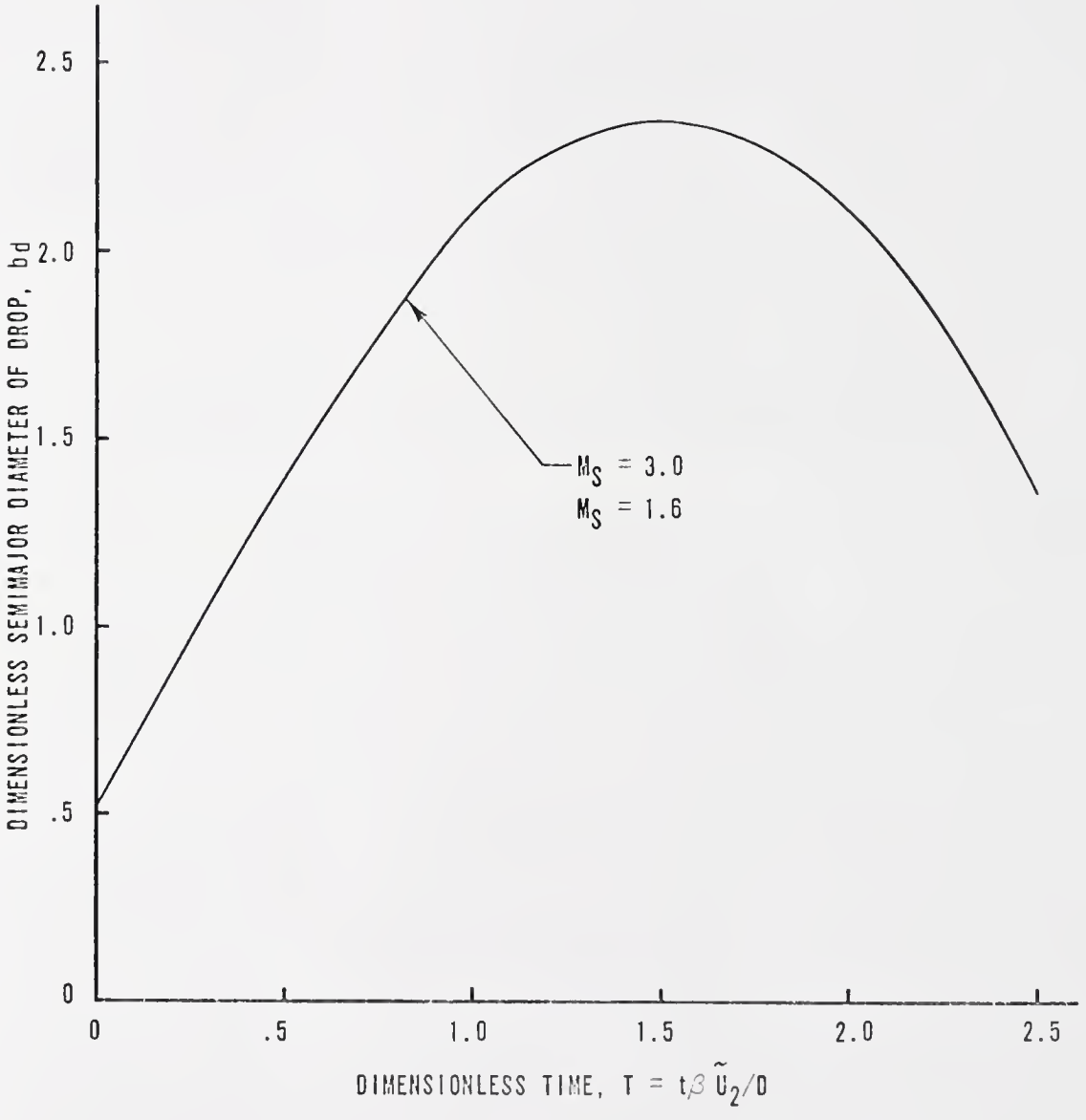

FIGURE 25. MEASURED SEMI-MAJOR DIAMETER OF THE DROP

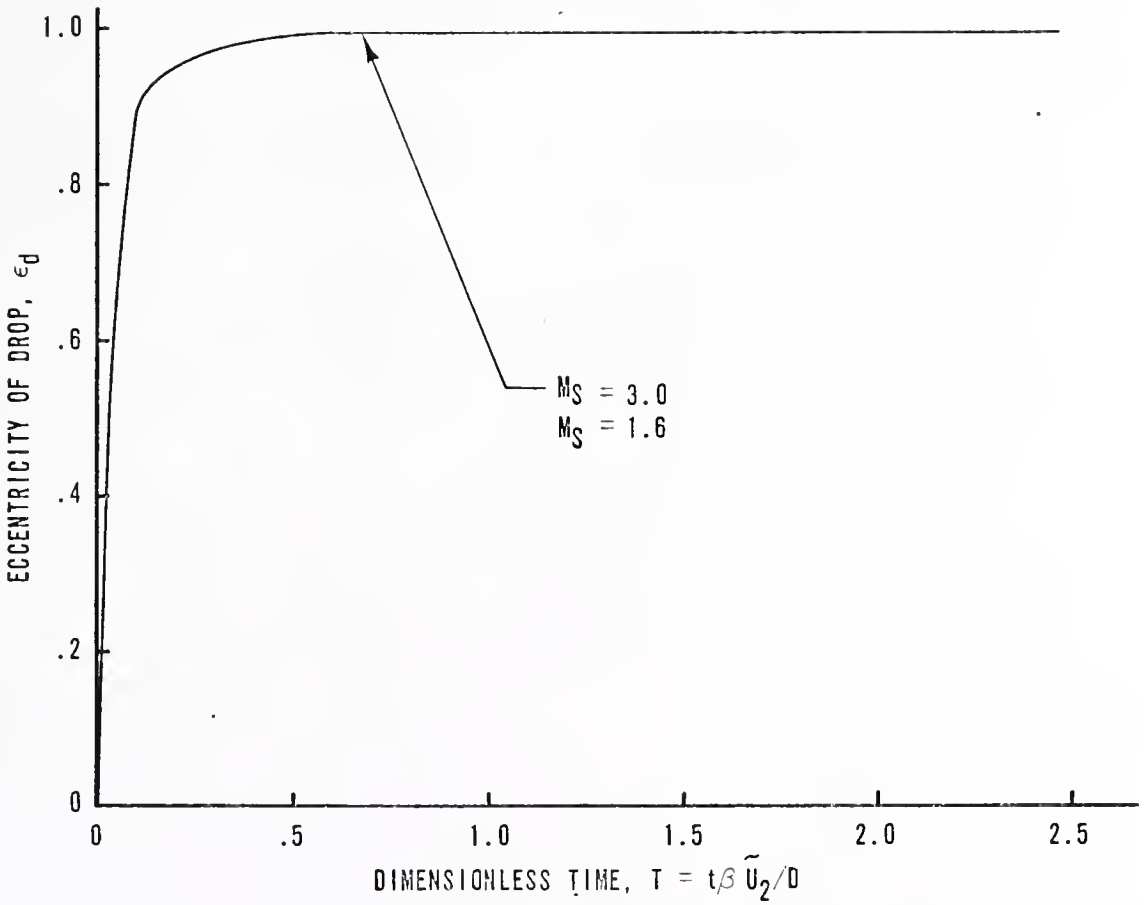

FIGURE 26. EXPERIMENTALLY DETERMINED ECCENTRICITY OF THE DROP

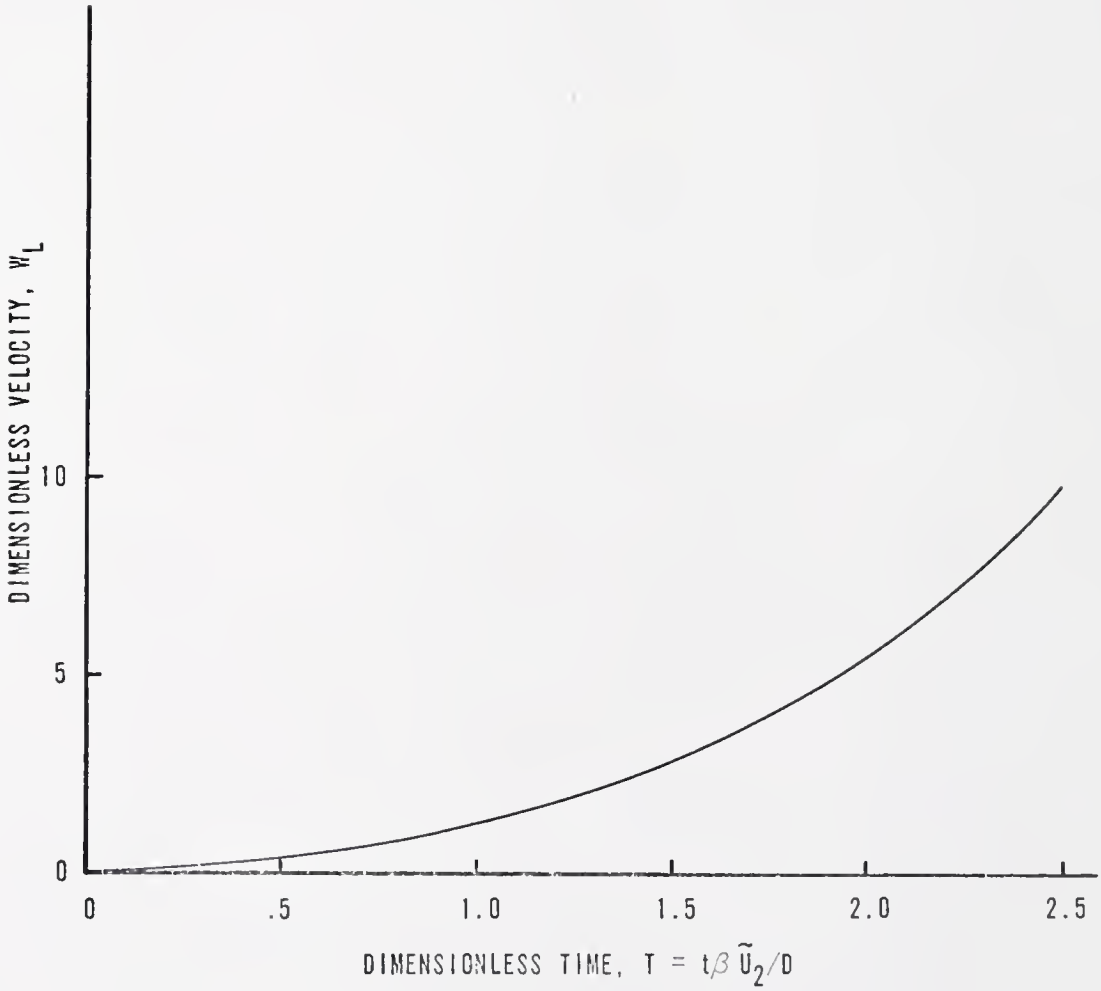

FIGURE 27. EXPERIMENTALLY DETERMINED VELOCITY OF THE STAGNATION POINT OF THE DROP

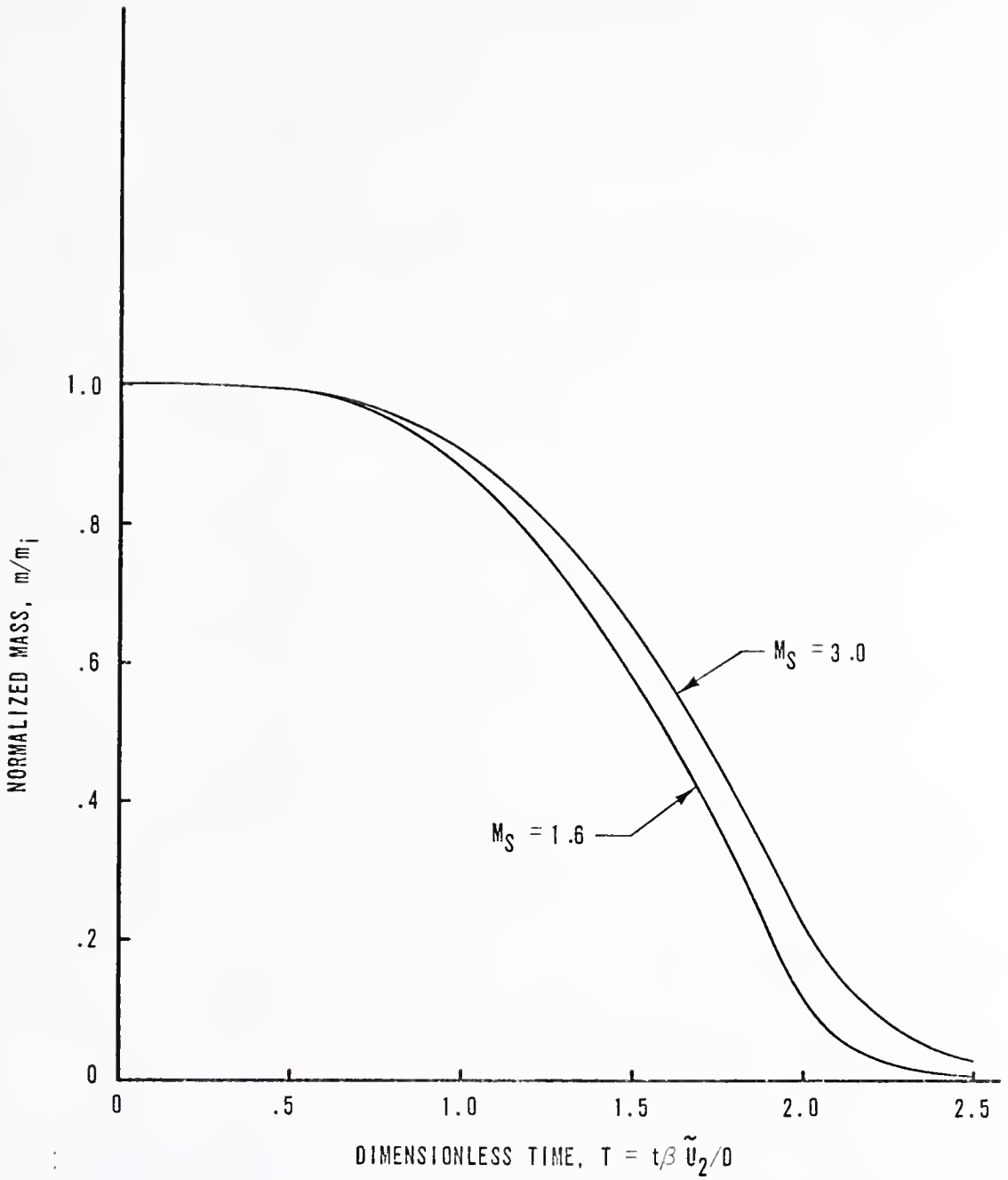

FIGURE 28. EXPERIMENTALLY DETERMINED NORMALIZED MASS OF THE DROP

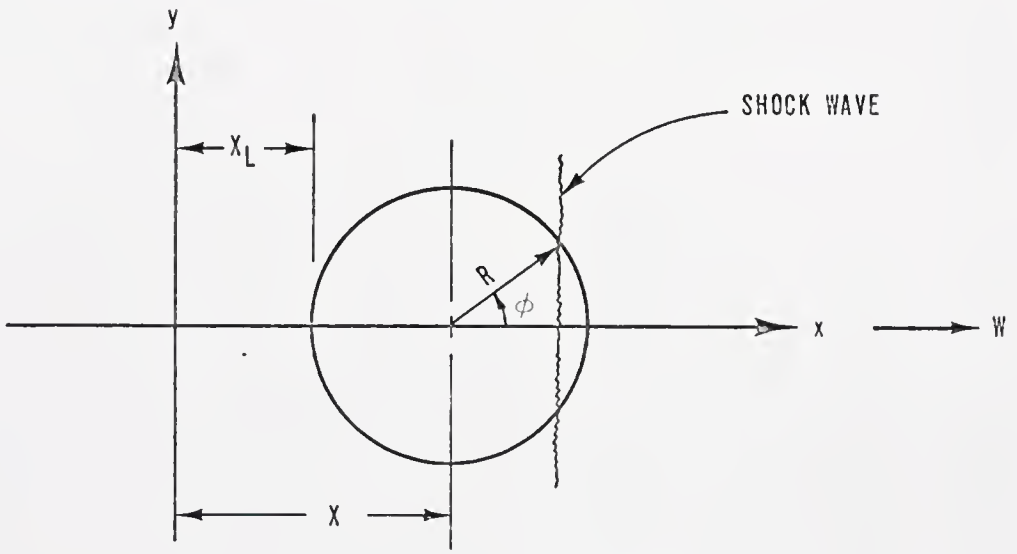

FIGURE 29. COORDINATE SYSTEMS FOR ANALYSIS OF SHOCK WAVE PASSAGE OVER THE DROP

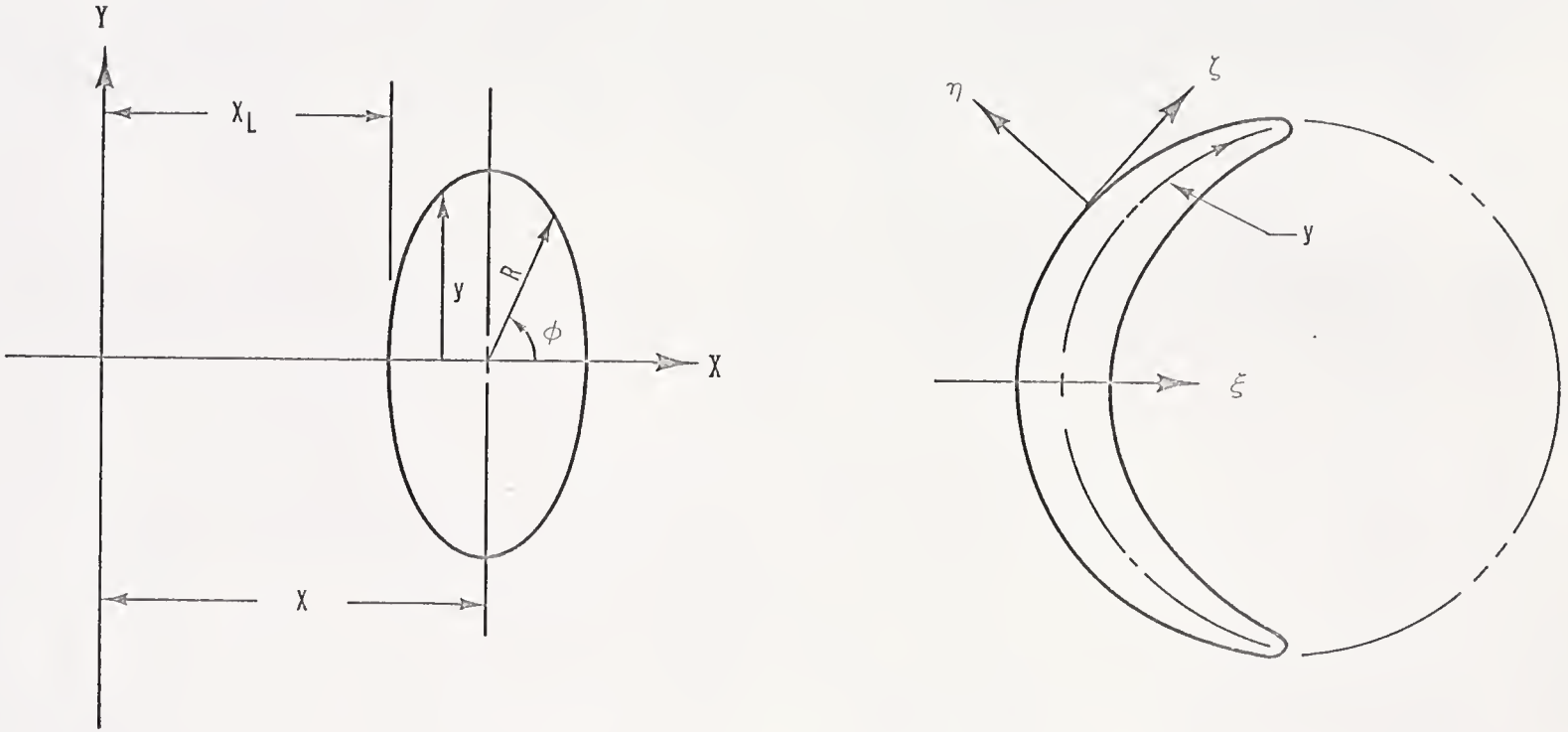

FIGURE 30. COORDINATE SYSTEMS FOR ANALYSIS OF DROP DEFORMATION AND FRAGMENTATION

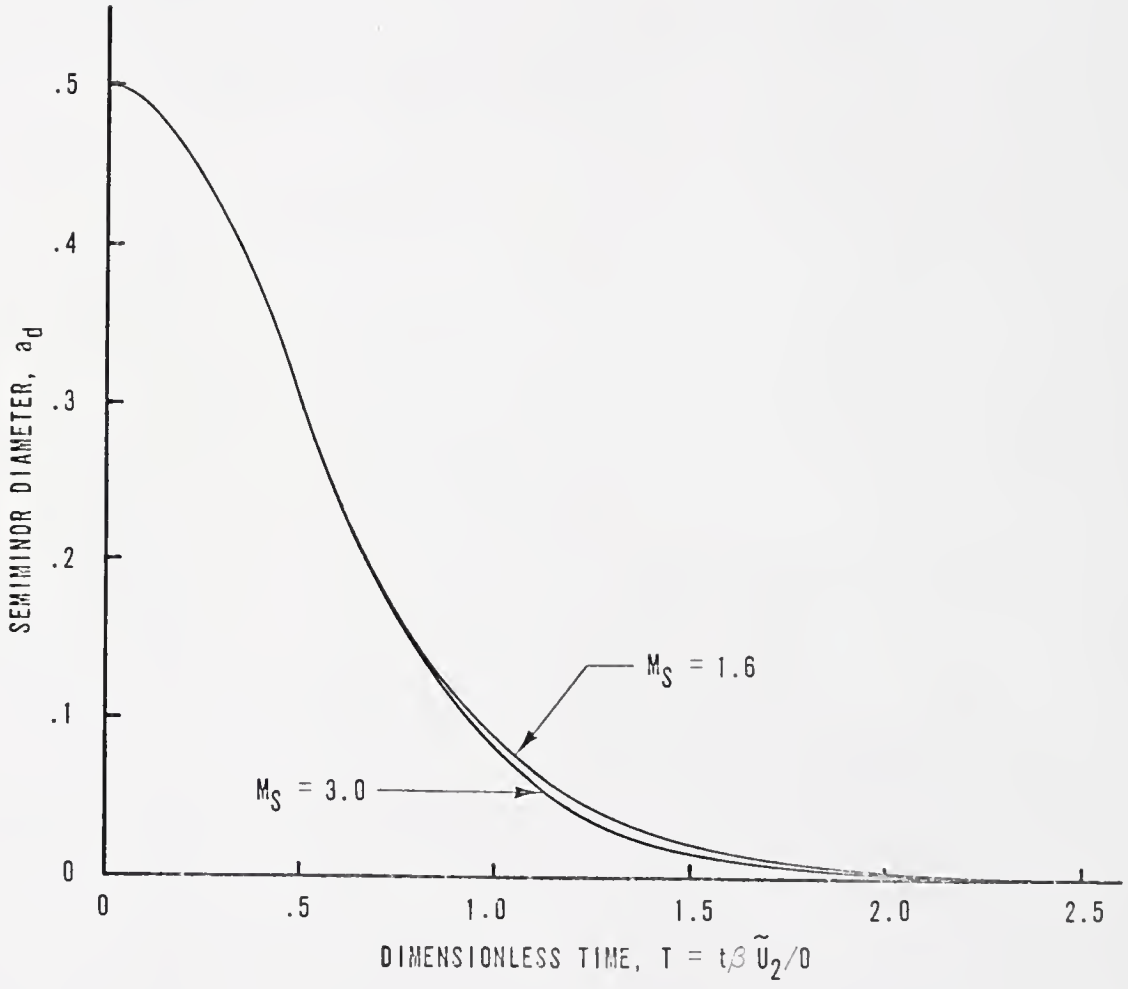

FIGURE 31. THEORETICAL SEMI-MINOR DIAMETER OF THE DROP

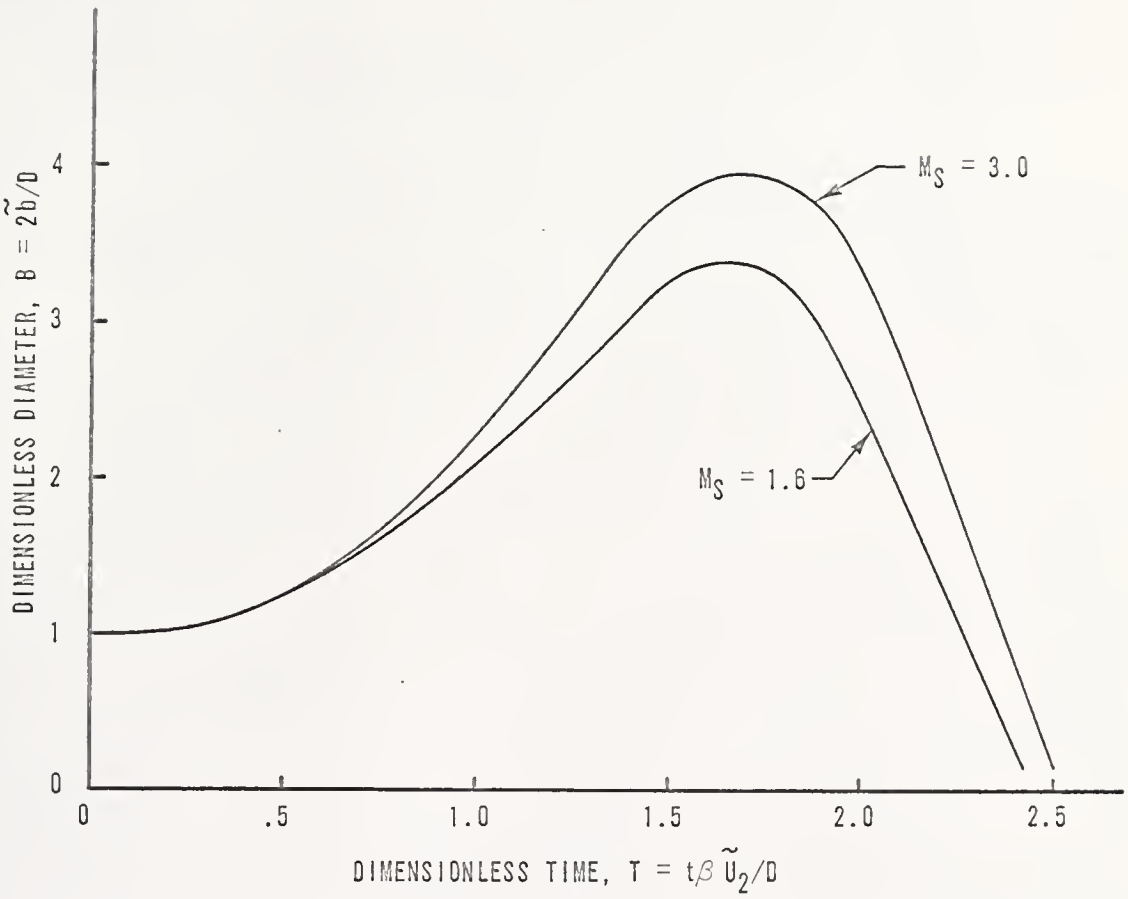

FIGURE 32. THEORETICAL MAJOR DIAMETER OF THE FRONTAL SURFACE OF THE DROP

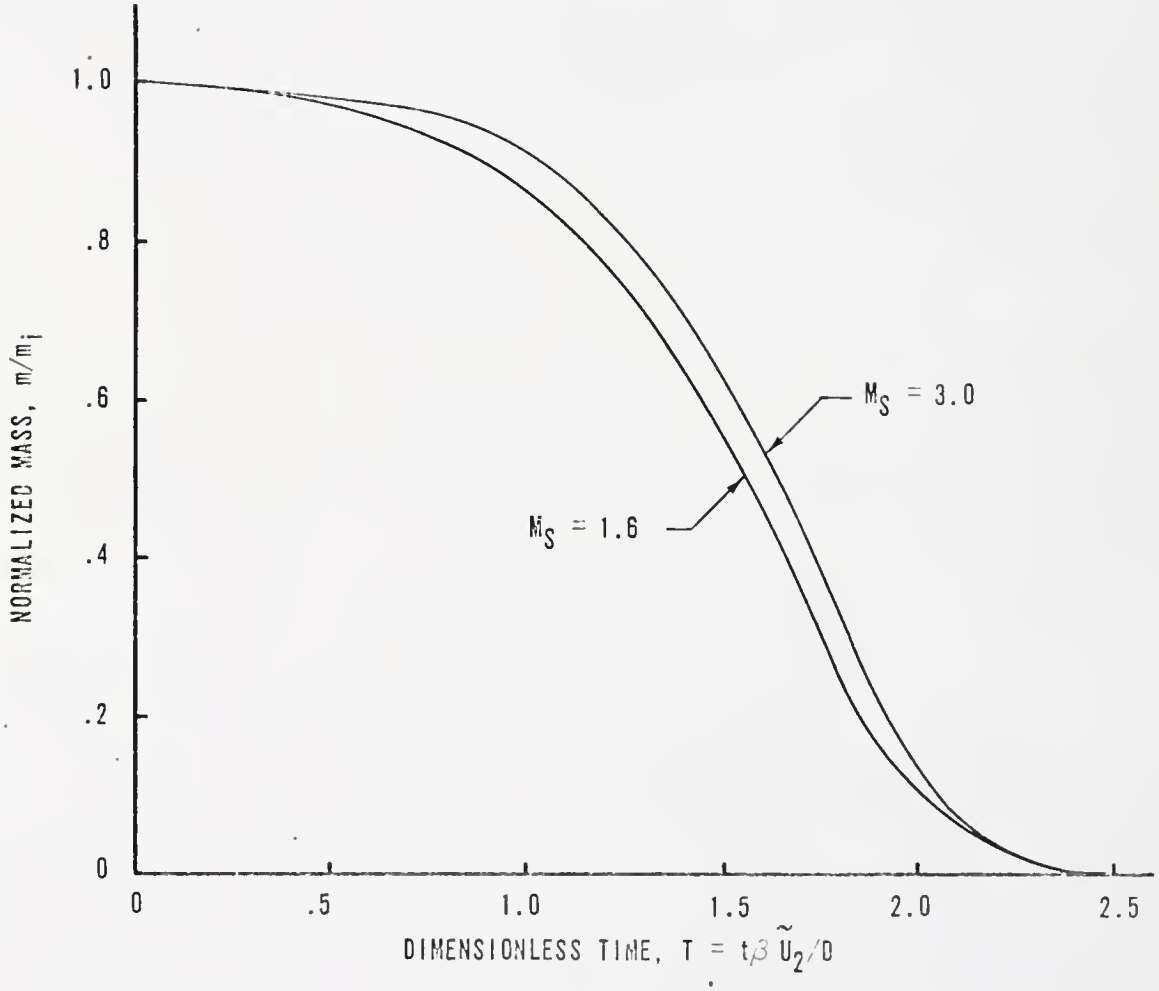

FIGURE 33. THEORETICAL NORMALIZED MASS OF THE DROP

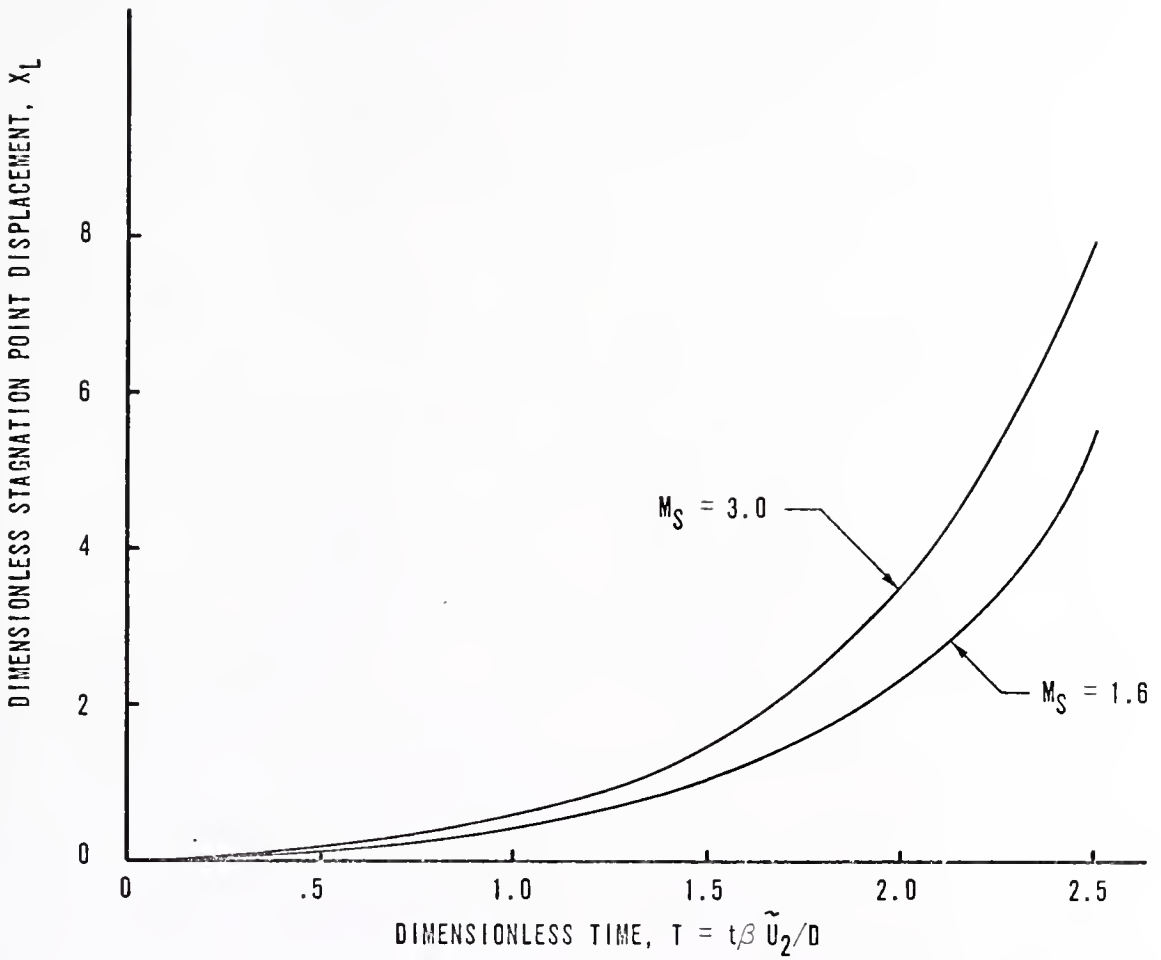

FIGURE 34. THEORETICAL DISPLACEMENT OF THE STAGNATION POINT OF THE DROP

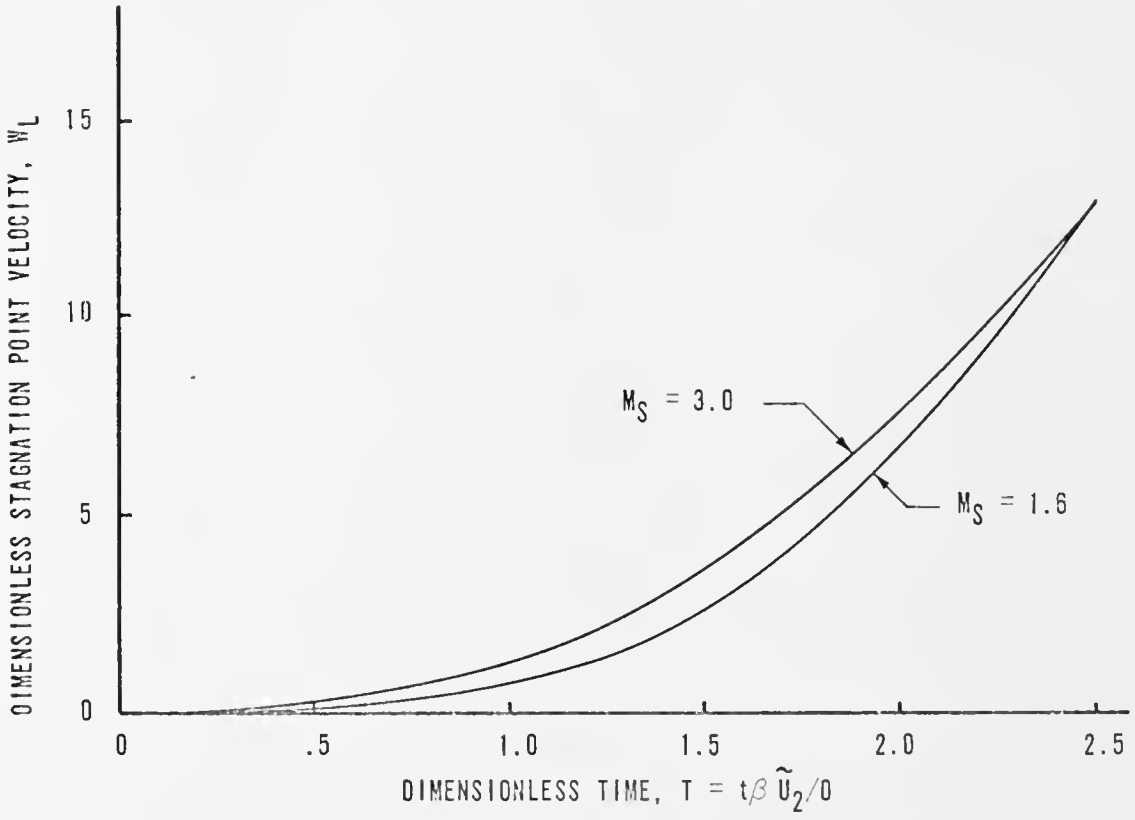

FIGURE 35. THEORETICAL VELOCITY OF THE STAGNATION POINT OF THE DROP

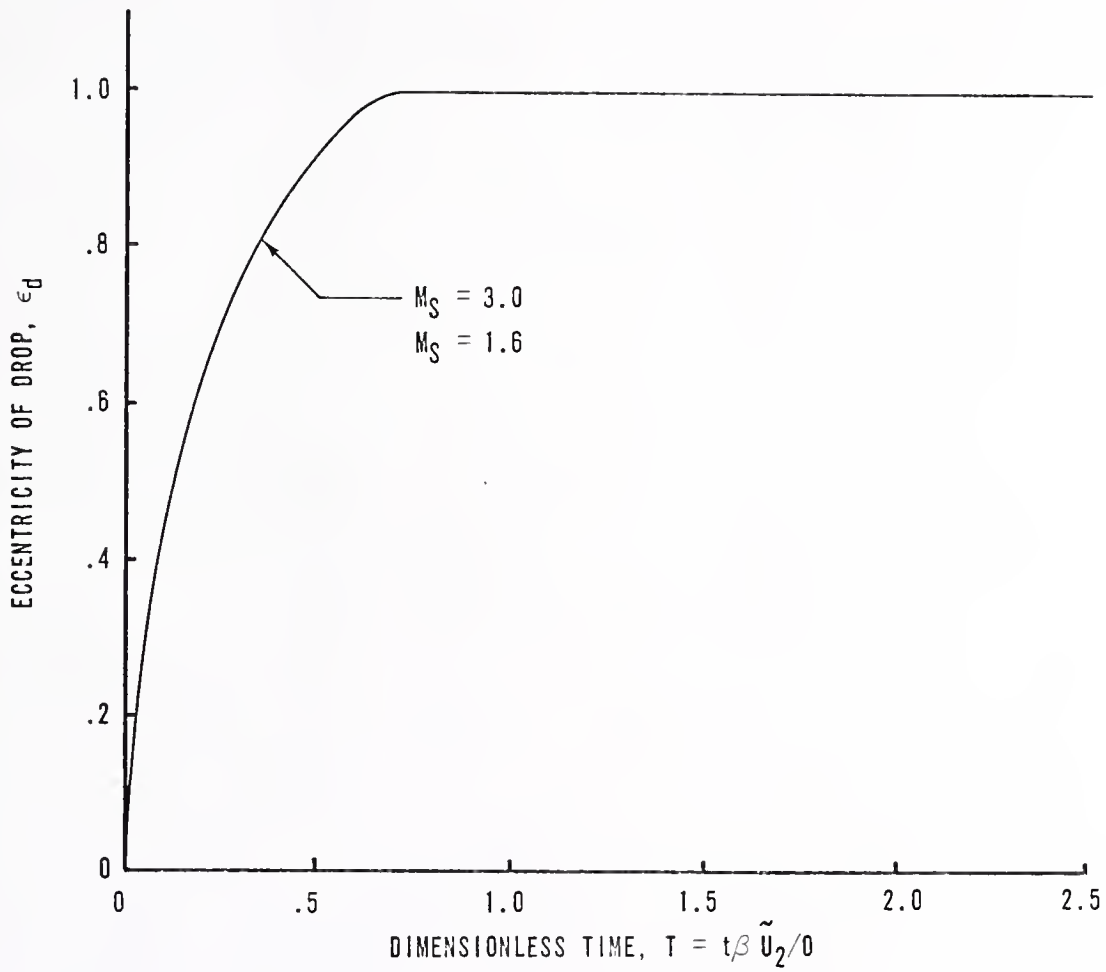

FIGURE 36. THEORETICAL ECCENTRICITY OF THE DROP

APPENDIX I

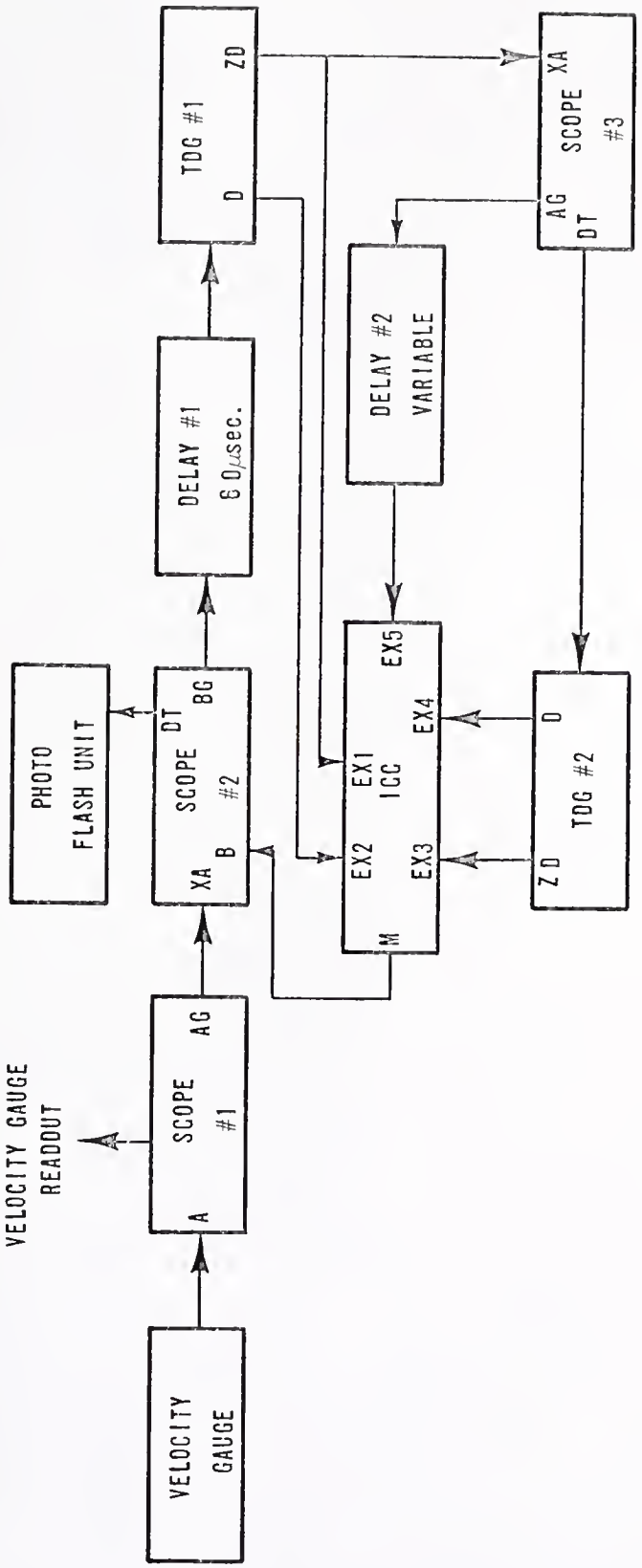

XA – A BEAM EXTERNAL TRIGGER
AG – A BEAM GATE
BG – B BEAM GATE
A – A BEAM INPUT
B – B BEAM INPUT
DT – DELAYED TRIGGER

TDG – TRW DELAY TRIGGER GENERATOR
D – DELAYED OUTPUT
ZD – ZERO DELAY OUTPUT
ICC – IMAGE CONVERTER CAMERA
EX – EXTERNAL TRIGGER PULSE INPUT
M – MONITOR OUTPUT PULSE

FIGURE 37. TIMING CIRCUIT SCHEMATIC

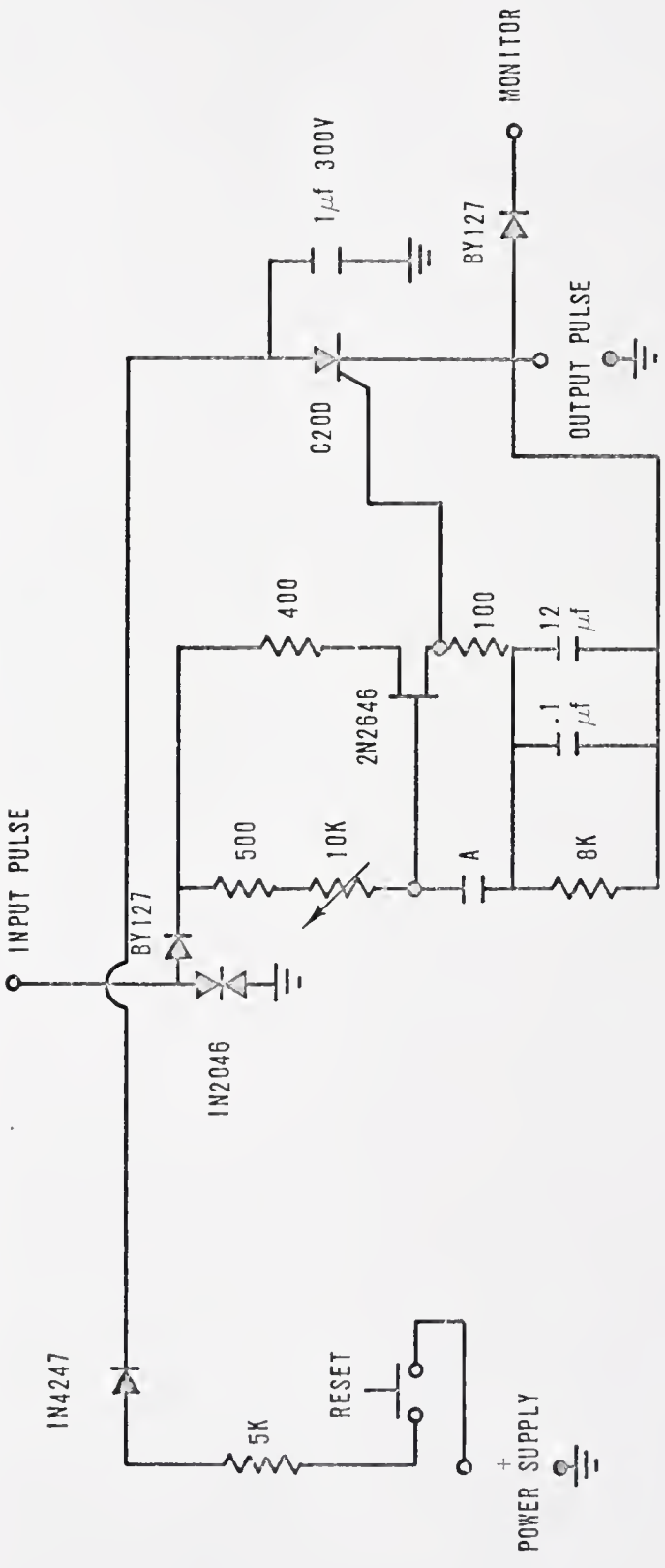

FIGURE 38. DELAY CIRCUIT SCHEMATIC

APPENDIX II

BOUNDARY LAYER STRIPPING ANALYSIS

The analysis for mass loss from the boundary layer on a spherical drop is attributable to Taylor.[5] The analysis presented here follows Taylor but is more general in that it applies to axisymmetric bodies.

Upon sudden exposure of a water drop to a high speed air stream boundary layers will form both in the air and in the water. The coordinate system used is shown in Figure 30 where ζ is the curvilinear coordinate along the interface separating the two fluids and η is the coordinate perpendicular to it and is taken positive in either direction from the interface. An approximate solution to this double boundary layer problem is obtained by assuming arbitrary simple velocity distributions containing several unknown parameters which are determined through use of Karman's momentum integral relations. Assume that the flow is steady and incompressible and that for the gas

$$\frac{u_2}{U_e} = 1 - (1 - U_I) \exp\left\{\frac{-\eta}{\alpha_2 \sqrt{\zeta}}\right\} \qquad \text{(AII-1)}$$

and for the water

$$\frac{u_\ell}{U_e} = U_I \exp\left\{\frac{-\eta}{\alpha_\ell \sqrt{\zeta}}\right\} \qquad \text{(AII-2)}$$

where, U_e is the local velocity in the gas outside of the boundary layer, U_I is a function of ζ and α_2 and α_ℓ are constants. The steady state boundary layer momentum integral

equations are for the gas

$$\frac{\partial}{\partial \xi}\int_0^\infty u_2(U_\ell - u_2)d\eta + \frac{1}{r}\frac{dr}{d\xi}\int_0^\infty u_2(U_\ell - u_2)\,d\eta + \frac{dU_\ell}{d\xi}\int_0^\infty (U_\ell - u_2)\,d\eta = \frac{\tau_{\eta=0}}{\rho_2} \tag{AII-3}$$

and for the water

$$\frac{\partial}{\partial \xi}\int_0^\infty u_\ell^2\,d\eta + \frac{1}{r}\frac{dr}{d\xi}\int_0^\infty u_\ell^2\,d\eta = -\frac{\tau_{\eta=0}}{\rho_\ell} + \frac{\rho_2}{\rho_\ell}U_\ell\frac{dU_\ell}{d\xi}\int_0^\infty d\eta \tag{AII-4}$$

where the pressure gradient in the liquid layer is given by

$$\frac{dp}{d\xi} = -\rho_2 U_\ell \frac{dU_\ell}{d\xi} \tag{AII-5}$$

At the gas-water interface the shear stresses must be equal and therefore

$$-\mu_\ell\left(\frac{\partial u_\ell}{\partial \eta}\right)_{\eta=0} = \mu_2\left(\frac{\partial u_2}{\partial \eta}\right)_{\eta=0} \tag{AII-6}$$

Applying equations (AII-1), (AII-2), and (AII-6) and evaluating the result at $\phi = \pi/2$ where for a sphere

$$\frac{dU_e}{d\zeta} = \frac{dr}{d\zeta} = 0$$

equations (AII-3) and (AII-4) become, respectively,

$$\frac{(1-U_I^2)\alpha_2 U_e^2}{4\sqrt{\zeta}} - \frac{U_e(1-U_I)\nu_2}{\alpha_2\sqrt{\zeta}} = 0 \qquad \text{(AII-7)}$$

and

$$\frac{(U_e U_I)^2 \alpha_e}{4\sqrt{\zeta}} - \frac{U_e U_I \nu_e}{\alpha_e\sqrt{\zeta}} = 0 \qquad \text{(AII-8)}$$

where ν is the kinematic viscosity coefficient.

These equations yield directly

$$\alpha_e = \left\{4\nu_e / U_I U_e\right\}^{1/2} \qquad \text{(AII-9)}$$

and

$$\alpha_2 = \left\{4\nu_2 / (U_I+1)U_e\right\}^{1/2} \qquad \text{(AII-10)}$$

Differentiating equations (AII-1) and (AII-2) with respect to η, inserting the result into equation (AII-6) and evaluating at $\eta = 0$, the following equation is obtained:

$$1-U_I-U_I^2+U_I^3(1-\beta^{-4}R_\mu^{-1})=0 \qquad \text{(AII-11)}$$

Since U_I is the interface velocity and is expected to be very small, equation (AII-11) can be approximated by:

$$1-U_I^3\beta^{-4}R_\mu^{-1}\approx 0 \qquad \text{(AII-12)}$$

and the interface velocity is

$$U_I=\beta^{4/3}R_\mu^{1/3} \qquad \text{(AII-13)}$$

The mass of water in the surface layer being swept along by the gas stream at a distance equal to the arc length between the stagnation point and the equator is given by

$$\frac{dm}{d\tau}=2\pi b\int_0^\infty u_l\,d\eta \qquad \text{(AII-14)}$$

where u_l is taken to be the local velocity as given by equation (AII-2) modified by a drop distortion velocity, U_d, due to internal flow within the drop. Hence

$$u_\ell = v_d + v_I v_\ell \exp\left\{\frac{-\eta}{\alpha\sqrt{\xi}}\right\} \qquad \text{(AII-15)}$$

The distortion velocity U_d is assumed to be proportional to the velocity of the fluid in the drop at the equatorial point such that

$$U_d = .065v$$

where v is given by equation (III-7b) and .065 is an empirical correlation factor. Equation (AII-14) can be written as

$$\frac{dm}{d\tau} = 2\pi b\left[.065\int_0^{\delta} v\,d\eta + \int_0^{\infty} v_I v_\ell \exp\left\{\frac{-\eta}{\alpha_\ell\sqrt{\xi}}\right\}d\eta\right] \qquad \text{(AII-16)}$$

where the first integral is taken over the boundary layer thickness, δ, defined such that

$$\exp\left\{\frac{-\delta}{\alpha_\ell\sqrt{\xi}}\right\} = .01$$

Performing the integrations indicated in equation (AII-16) there results

$$\frac{dm}{d\tau} = 2\pi b\left\{.065 v\delta + \left(\frac{\pi b}{2}\right)^{1/2} v_\ell v_I \alpha_\ell\right\} \qquad \text{(AII-17)}$$

Integrating equation (AII-17) over a small time interval, Δ T, so that all time dependent parameters can be considered constant with negligible error and applying equations (AII-9) and (AII-13) to the result the mass loss from the drop is found to be

$$\Delta m_i = -(2\pi b_{i-1})^{3/2} K_4 \beta^{5/6} R_\mu^{-1/3} (1-\beta W)^{1/2} \nu_2^{1/2} \Delta T_i$$
$$-.065\pi b_{i-1} S_i (f_i + f_{i-1}) \Delta T_i \qquad \text{(AII-18)}$$

The local velocity, U_ℓ, at the equator of the drop is approximated by

$$U_\ell = K_4^2 (1-\beta W)/\beta \qquad \text{(AII-19)}$$

Equation (AII-19) is based on the assumption of isentropic flow around the drop. This assumption is of course not strictly valid for supersonic flow; however, since $M_R \leq 1.35$ for the present study, the entropy change is small and the assumption of isentropic flow introduces little error. For subsonic incompressible flow, $M_R < 0.7$, the velocity at the equator of the drop[14] is

$$U_\ell = 1.5 (1-\beta W)/\beta$$

and for supersonic flow with $M_R > 1.3$

$$U_\ell = (1-\beta W)/\beta$$

In the Mach number range, $.7 \leq M_R \leq 1.3$ K_4 is assumed to vary linearly and is given by

$$K_4 = 1.1125 - 0.1875\left(|M_R - .7| - |M_R - 1.3|\right)$$

The velocity, W_i, appearing in equations (AII-18) and (AII-19) is the velocity of the drop assuming no deformation is occurring and is given by equation (III-4) with:

$$\alpha_i = \frac{\pi b_{i-1}^2 (\rho_z C_{pm})}{m_{i-1}} \left\{ 1 - K_3 - .5 K_1 \right\}_i \qquad \text{(AII-20)}$$

APPENDIX III

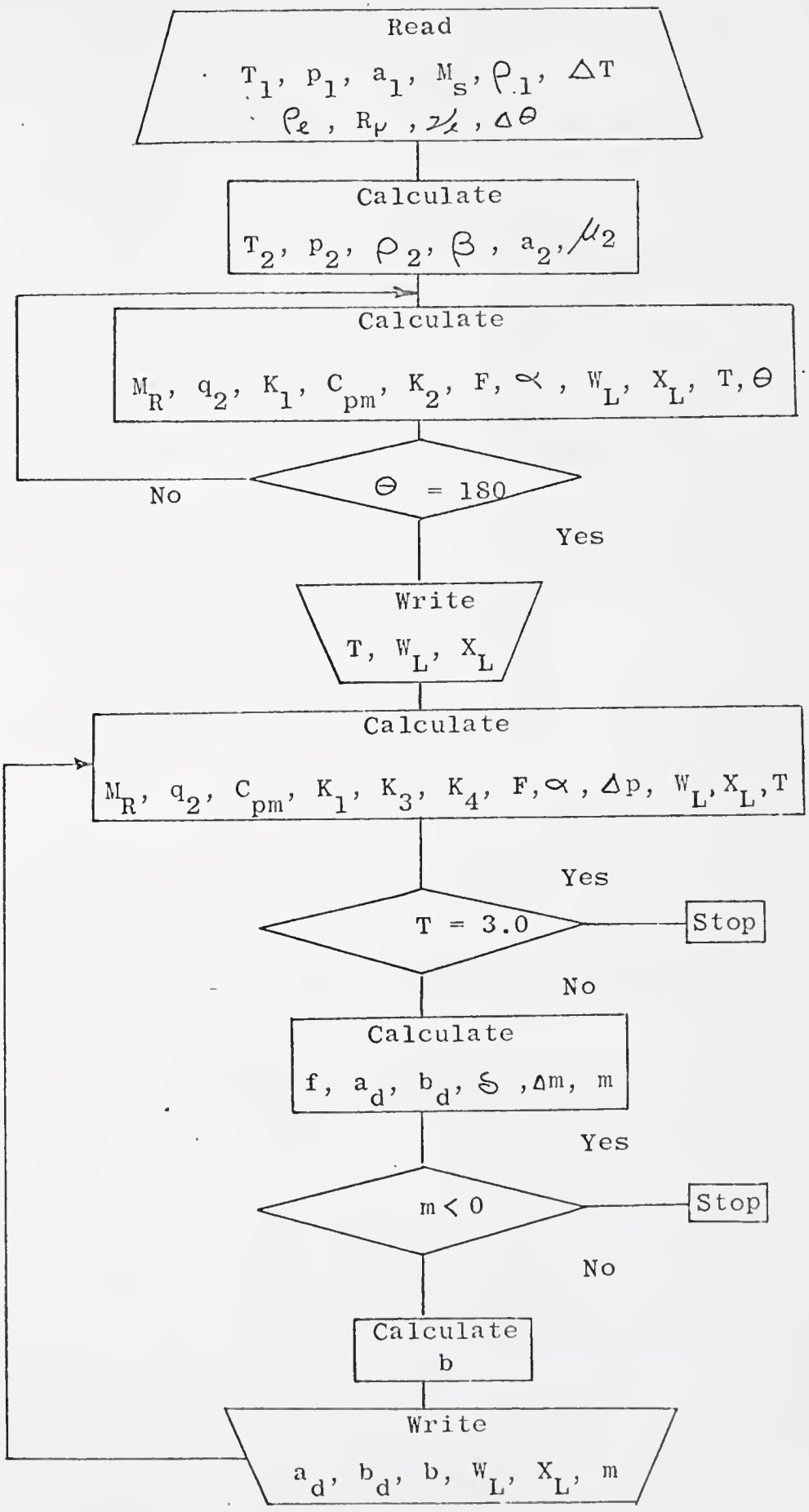

FIGURE 39. COMPUTER PROGRAM FLOW CHART

REFERENCES

1. Engel, O. G., "Fragmentation of Water Drops in the Zone Behind an Air Shock," J. Res. N.B.S., 60, 245-280 (1958).

2. Hanson, A. R., Domich, E. G., and Adams, H. S., "Shock Tube Investigation of the Breakup of Drops by Air Blasts," Phys Fluids, 6, 1070-1080 (1963).

3. Nicholson, J. E. and Figler, B. D., "Complementary Aerodynamic Test Techniques for Rain Erosion Alleviation Studies," AIAA Paper, 66-766, September 1966.

4. Ranger, A. A., and Nicholls, J. A., "Aerodynamic Shattering of Liquid Drops," AIAA Journal, 7, 285-290 (1969).

5. Taylor, G. I., "The Shape and Acceleration of a Drop in a High Speed Air Stream," The Scientific Papers of G. I. Taylor, edited by G. K. Batchelor, III, 247-264, University Press, Cambridge (1963).

6. Clemons, J. F., An Experimental Investigation of Shock Phenomena in Argon, Thesis, University of Florida (1967).

7. Anonymous, TRW Model 1D Image Converter Camera Technical Manual, TRW Instruments, El Segundo, Calif. (1966).

8. Brunsvold, R. S., The Design and Construction of a Platinum Film Velocity Gauge, Thesis, University of Florida (1969).

9. Anonymous, TRW Model 46A Trigger Delay Generator Technical Manual, TRW Instruments, El Segundo, Calif. (1966).

10. Anonymous, Type 556/R556 Oscilloscope Instruction Manual, Tektronix, Inc., Beaverton, Oregon (1966).

11. Strutt, J. D., Lord Rayleigh, Theory of Sound, Dover Publications, Inc., New York (1945).

12. Schlichting, H., Boundary Layer Theory, McGraw-Hill Book Company, Inc., New York (1960).

13. Anonymous, Handbook of Supersonics, NAVWEPS Report 1488, 3, 66 (1961).

14. Milne - Thomson, L. M., Theoretical Hydrodynamics, Macmillan Company, New York (1968).

BIOGRAPHICAL SKETCH

William Edward Krauss was born May 12, 1928, at Cleveland, Ohio. He was graduated from East Technical High School in Cleveland in 1946. In September, 1950, he received the degree of Bachelor of Mechanical Engineering from the Ohio State University. Upon graduation he was employed by United States Steel Corporation and then North American Aviation, Inc. In October, 1952, he returned to the Ohio State University and in June, 1953, he received the Master of Science degree. He was a research associate with the Ohio State University Research Foundation until 1954 when he was employed by Convair in Fort Worth, Texas. From February, 1959, until the present he has been employed by the Martin Marietta Corporation, Orlando, Florida, in various engineering staff and management positions. He is currently assigned as division staff engineer for the Aeromechanical Division.

William Edward Krauss is married to the former Barbara Allen Marlin and is the father of two children. He is a registered professional engineer in Texas and Ohio and an Associate Fellow of the American Institute of Aeronautics and Astronautics.

This dissertation was prepared under the direction of the chairman of the candidate's supervisory committee and has been approved by all members of that committee. It was submitted to the Dean of the College of Engineering and to the Graduate Council, and was approved as partial fulfillment of the requirements for the degree of Doctor of Philosophy.

June, 1970

Robert E Uhrig

Dean, College of Engineering

Dean, Graduate School

Supervisory Committee:

F M Deaton

Chairman

M. H. Chaudhry

D. D. Williams

K. R. McCrum

R. G. Blake

Karl Pohlhausen